

High-spin structures of $^{124-131}\text{Te}$: Competition of proton and neutron pair breakings

A. Astier,¹ M.-G. Porquet,¹ Ts. Venkova,^{1,2} Ch. Theisen,³ G. Duchêne,^{4,5} F. Azaiez,^{4,5,*} G. Barreau,⁶ D. Curien,^{4,5} I. Deloncle,¹ O. Dorvaux,^{4,5} B.J.P. Gall,^{4,5} M. Houry,^{3,†} R. Lucas,³ N. Redon,⁷ M. Rousseau,^{4,5} and O. Stézowski⁷

¹CSNSM, IN2P3-CNRS and Université Paris-Sud, Bât 104-108, F-91405 Orsay, France

²INRNE, BAS, 1784 Sofia, Bulgaria

³CEA, Centre de Saclay, IRFU/Service de Physique Nucléaire, F-91191 Gif-sur-Yvette Cedex, France

⁴Université de Strasbourg, IPHC, 23 rue du Loess, F-67037 Strasbourg, France

⁵CNRS, UMR7178, F-67037 Strasbourg, France

⁶CENBG, IN2P3-CNRS and Université Bordeaux I, F-33175 Gradignan, France

⁷IPNL, IN2P3-CNRS and Université Claude Bernard, F-69622 Villeurbanne Cedex, France

(Dated: December 18, 2013)

The $^{124-131}\text{Te}$ nuclei have been produced as fission fragments in two fusion reactions induced by heavy-ions ($^{12}\text{C} + ^{238}\text{U}$ at 90 MeV bombarding energy and $^{18}\text{O} + ^{208}\text{Pb}$ at 85 MeV) and studied with the Euroball array. Their high-spin level schemes have been extended to higher excitation energy from the triple γ -ray coincidence data. The $\gamma - \gamma$ angular correlations have been analyzed in order to assign spin and parity values to many observed states. Moreover the half-lives of isomeric states have been measured from the delayed coincidences between the fission-fragment detector SAPHIR and Euroball, as well as from the timing information of the Ge detectors. The behaviors of the yrast structures identified in the present work are first discussed in comparison with the general features known in the mass region, particularly the breakings of neutron pairs occupying the $\nu h_{11/2}$ orbit identified in the neighboring Sn nuclei. The experimental level schemes are then compared to shell-model calculations performed in this work. The analysis of the wave functions shows the effects of the proton-pair breaking along the yrast lines of the heavy Te isotopes.

PACS numbers: 23.20.Lv, 21.60.Cs, 27.60.+j, 25.85.Ge

I. INTRODUCTION

The experimental study of nuclei around the doubly-magic ^{132}Sn nucleus is of special interest. Such new data allow us to test ingredients of shell-model (SM) calculations far away from the valley of stability. For instance, a realistic effective interaction to be used in the 50 – 82 valence shell was derived from the CD-Bonn nucleon-nucleon potential and has been tested in several nuclei having few proton particles and neutron holes away from the doubly-magic core: $^{134}\text{Te}_{82}$, $^{130}\text{Sn}_{80}$, $^{132}\text{Sb}_{81}$ and $^{132}\text{Te}_{80}$ [1]. The experimental energy levels of these four nuclei are well reproduced showing that such an approach for determining the two-body matrix elements could provide an accurate description of nuclear structure properties. More recently, the experimental high-spin states of five $N = 82$ isotones [2] were described using this interaction [3], named SN100PN. Nevertheless because of their neutron magic number, only the proton parts of the interaction take place in such SM calculations. In order to assess more precisely the quality of this realistic effective interaction, the results of SM calculations have to be compared to experimental data in other nuclei. For instance all the parts of the effective interaction can be tested using nuclei having neutron holes in presence of

a few proton particles, such as the ^{52}Te isotopes with $N < 80$.

Yrast excitations in several heavy-mass Te isotopes have been already experimentally obtained using deep-inelastic reactions, the states of $^{127-131}\text{Te}$ being identified up to spin (23/2) and those of $^{126,128}\text{Te}$ up to spin (12) or (14) [4], i.e., up to the breaking of the first $\nu h_{11/2}$ pair. More recently, a new level scheme of ^{130}Te has been established, showing an isomeric state at 4.4 MeV excitation energy [5]. The use of binary fission induced by heavy ions allows us to extend the yrast line to higher-spin states, particularly those coming from the breaking of several pairs.

Thus, in this work, the $^{124-131}\text{Te}$ isotopes have been produced as fragments of two fusion-fission reactions. Their level schemes have been built from the γ high-fold events and $\gamma - \gamma$ angular correlations have been analyzed in order to assign spin and parity values to most of the states. In addition, the half-lives of isomeric states have been measured from the delayed coincidences between a fission fragment detector and the gamma array, or from the timing of the Ge detectors. Several Te isotopes with heavier masses were also observed in the C+U reaction. The identification of their complementary fragments by means of the cross coincidences of their γ -rays indicates that they are not produced from the same reaction channel as $^{124-131}\text{Te}$, but from fissions following transfer or incomplete fusion. Many other nuclei belonging to the $A \sim 140 - 144$ region have also singular partners, implying that they are produced from the same mechanism.

In the last part of this paper, all the yrast states of

* Present address: IPNO, IN2P3-CNRS and Université Paris-Sud, F-91406 Orsay, France

† Present address: CEA/DSM/Département de recherches sur la Fusion Contrôlée, F-13108 Saint-Paul lez Durance, France

$^{124-131}\text{Te}$ are firstly discussed in comparison with the general features known in this mass region. The predictions from SM calculations using the SN100PN effective interaction [1] then are presented, starting from the description of the high-spin states of several Sn isotopes in which the breakings of several neutron pairs occupying the $\nu h_{11/2}$ orbit were experimentally identified [6–8]. With regard to the Te isotopes, the SM calculations are done in the full valence space in four cases, $^{128-131}\text{Te}$ and the theoretical predictions are compared to the experimental results. In addition, the detailed analysis of the wave functions of the high-spin states shows the effects of the proton-pair breaking along the yrast lines of the heavy Te isotopes.

II. EXPERIMENTAL DETAILS

A. Reactions, γ -ray detection and analysis

The ^{52}Te isotopes of interest were obtained as fission fragments in two experiments. First, the $^{12}\text{C} + ^{238}\text{U}$ reaction was studied at 90 MeV incident energy, with a beam provided by the Legnaro XTU Tandem accelerator. Second, the $^{18}\text{O} + ^{208}\text{Pb}$ reaction was studied with a 85 MeV incident energy beam provided by the Vivitron accelerator of IReS (Strasbourg). The γ rays were detected with the Euroball array [9]. The spectrometer contained 15 cluster germanium detectors placed in the backward hemisphere with respect to the beam, 26 clover germanium detectors located around 90° and 30 tapered single-crystal germanium detectors located at forward angles. Each cluster detector consists of seven closely packed large-volume Ge crystals [10] and each clover detector consists of four smaller Ge crystals [11]. In order to get rid of the Doppler effect, both experiments have been performed with thick targets in order to stop the recoiling nuclei (47 mg/cm² for ^{238}U and 100 mg/cm² for ^{208}Pb targets, respectively).

The data of the C+U experiment were recorded in an event-by-event mode with the requirement that a minimum of five unsuppressed Ge detectors fired in prompt coincidence. A set of 1.9×10^9 three- and higher-fold events was available for a subsequent analysis. For the O+Pb experiment, a lower trigger condition (three unsuppressed Ge) allowed us to register 4×10^9 events with a γ -fold greater than or equal to 3. The offline analysis consisted of both multigated spectra and three-dimensional 'cubes' built and analyzed with the Radware package [12].

More than one hundred nuclei are produced at high spin in such experiments, and this gives several thousands of γ transitions which have to be sorted out. Single-gated spectra are useless in most of the cases. The selection of one particular nucleus needs at least two energy conditions, implying that at least two transitions have to be known. It is worth noting that prompt γ rays emitted by couples of complementary fragments are detected in

coincidence [13, 14]. Because the isotopes of interest are produced from two different fissioning compound nuclei in this work, the complementary fragments are different in the two reactions. This gives a fully unambiguous assignment of transitions seen in both experiments.

The relative intensity of the lowest transitions of the even- A Te isotopes have been measured in spectra in double coincidences with two transitions emitted by one partner. Then, we have used the spectra in double coincidences with one low-lying transition of the Te isotope of interest and one transition of a partner. Finally, for determining the intensity of the weak transitions, we have analyzed spectra in double coincidences with two transitions of the Te level schemes and normalized the obtained results by using relative intensities extracted from the spectra mentioned above.

B. Isomer identification

As reported in previous papers [2, 6, 15, 16], another experiment was performed using the SAPHIR¹ heavy-ion detector [17], here composed of 32 photovoltaic cells, in order to identify new isomeric states in the fission fragments. Placed in the target chamber of Euroball, SAPHIR was used to detect the escaping fission-fragments of the $^{12}\text{C} (90 \text{ MeV}) + ^{238}\text{U}$ reaction from a thin 0.14 mg/cm² uranium target. The detection of the two fragments in coincidence providing a clean signature of fission events was used as the trigger for Euroball. The Euroball time window was [50 ns–1 μ s], allowing detection of delayed γ -rays emitted during the de-excitation of isomeric states. Time spectra between fragments and γ -rays were analyzed in order to measure the half-life of isomeric levels, in a range of several tens to several hundreds of nanoseconds.

C. γ - γ angular correlations

It is well known that the γ rays emitted by fusion-fission fragments do not show any anisotropy in their angular distributions with respect to the incident beam. However, angular correlations of two successive transitions are meaningful. In order to determine the spin values of excited states, the coincidence rates of two successive γ rays are analyzed as a function of θ , the average relative angle between the two fired detectors. The Euroball spectrometer had $C_{239}^2=28441$ combinations of two crystals, out of which ~ 2000 involved different values of relative angle within 2° . Therefore, in order to keep reasonable numbers of counts, all these angles have been gathered around three average relative angles : 22° , 46° ,

¹ SAPHIR, Saclay Aquitaine Photovoltaic cells for Isomer Research.

and 75° . The coincidence rate increases between 0° and 90° for the dipole-quadrupole cascades, whereas it decreases for the quadrupole-quadrupole or dipole-dipole ones. The theoretical values of several coincidence rates for the Euroball geometry have been already given in previous papers [18–20]. The method has been checked by correctly reproducing the expected angular correlations of γ -transitions having well-known multipole orders and belonging to various fission fragments.

When the statistics of our data are too low to perform such a measurement, the spin assignments are based upon (i) the already known spins of some states, (ii) the assumption that in yrast decays, spin values increase with the excitation energy, (iii) the possible existence of cross-over transitions, and (iv) the analogy with the level structures of the other isotopes.

III. EXPERIMENTAL RESULTS

The γ -rays emitted by the low-lying states of $^{122-132}\text{Te}$ isotopes have been observed in both fusion-fission reactions used in the present work. Regarding ^{122}Te and ^{132}Te , their yield are so low that only the decays of their low-lying yrast states are observed and the transitions of their partners could not be identified in gated spectra. On the other hand, we have measured many new γ -rays emitted by the high-spin states of $^{124-131}\text{Te}$. The results are presented in the two following sections. In the third one, we discuss the particular cases of $^{133-136}\text{Te}$ which have been only observed in the $^{12}\text{C} + ^{238}\text{U}$ reaction.

A. Study of the even- A $^{124-130}\text{Te}$ isotopes

1. Level scheme of ^{124}Te

Previous information of the medium-spin excited states of ^{124}Te comes from results of the $(\alpha, 2n\gamma)$ reaction [21]. The positive-parity yrast band was identified up to the $I = 10^+$ state at 3152 keV and the negative-parity one up to the $I = 11^-$ state at 3987 keV. In addition, a $I = 11$ level was proposed at 3850 keV. We confirm the decay schemes of the 10^+ and 11^- states and we have added a few new states at higher energy (see the colored states in Fig. 1). We have gathered in Table I the properties of all the transitions assigned to ^{124}Te from this work.

The statistics of our ^{124}Te data is too low to perform $\gamma - \gamma$ angular correlation analyses. Therefore, the spin assignments of all the new states shown in Fig. 1 are based on close similarity with the results obtained in the other isotopes, which are presented in the following sections. It is worth noting that the angular distributions of the two transitions at 697 and 698 keV were measured in the previous work dealing with the $(\alpha, 2n\gamma)$ reaction [21]. While the latter exhibits the standard coefficients of a quadrupole transition, the extremely large value of the a_2 coefficient [$a_2 = 0.82(3)$] of the former led the authors

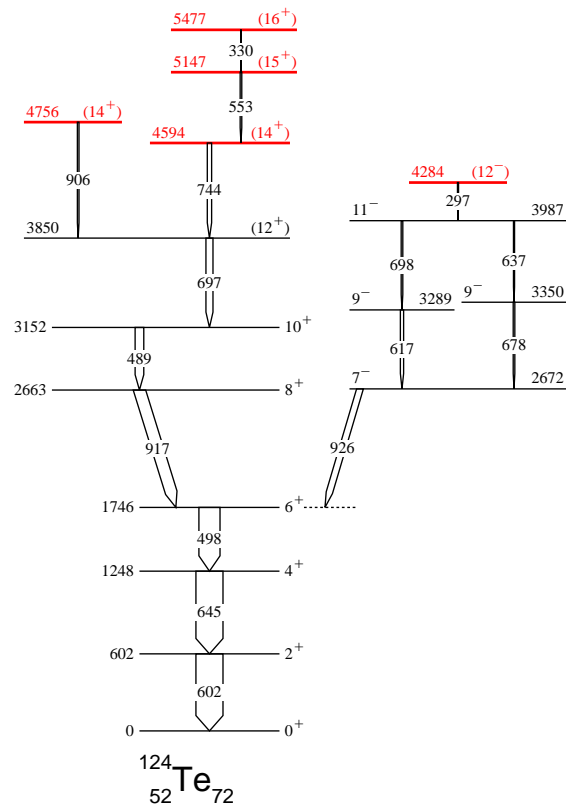


FIG. 1. (Color online) Level scheme of ^{124}Te deduced in the present work. The colored levels are new. The width of the arrows is proportional to the relative intensity of the γ rays.

TABLE I. Properties of the transitions assigned to ^{124}Te observed in this work.

$E_\gamma^{(a)}$ (keV)	$I_\gamma^{(a),(b)}$	$J_i^\pi \rightarrow J_f^\pi$	E_i	E_f
297.4(4)	4.1(16)	$(12^-) \rightarrow 11^-$	4284.5	3987.1
330.2(4)	2(1)	$(16^+) \rightarrow (15^+)$	5476.8	5146.6
489.5(3)	32(6)	$10^+ \rightarrow 8^+$	3152.4	2662.9
498.1(3)	77(12)	$6^+ \rightarrow 4^+$	1746.0	1247.9
553.1(4)	4.8(19)	$(15^+) \rightarrow (14^+)$	5146.6	4593.5
602.4(3)	-	$2^+ \rightarrow 0^+$	602.4	0.0
616.5(4)	11(3)	$9^- \rightarrow 7^-$	3288.7	2672.2
637.3(5)	4.4(18)	$11^- \rightarrow 9^-$	3987.1	3349.8
645.5(2)	100	$4^+ \rightarrow 2^+$	1247.9	602.4
677.6(5)	5.7(23)	$9^- \rightarrow 7^-$	3349.8	2672.2
697.3(3)	25(5)	$(12^+) \rightarrow 10^+$	3849.7	3152.4
698.5(4)	5.9(24)	$11^- \rightarrow 9^-$	3987.1	3288.7
743.8(4)	15(4)	$(14^+) \rightarrow (12^+)$	4593.5	3849.7
906.1(5)	4.7(19)	$(14^+) \rightarrow (12^+)$	4755.8	3849.7
916.9(3)	44(9)	$8^+ \rightarrow 6^+$	2662.9	1746.0
926.2(3)	23(5)	$7^- \rightarrow 6^+$	2672.2	1746.0

^(a) The number in parentheses is the error in the least significant digit shown.

^(b) The relative intensities are normalized to $I_\gamma(645) = 100$.

to assign a dipole character to the 697-keV transition

(implying a $I = 11$ value for the decaying state at 3850 keV, at variance with the $I = 12$ value proposed in the present work). Nevertheless it has to be noticed that these two transitions are also close in energy with the broad γ line at 697 keV emitted by the 2^+ state of ^{74}Ge , casting doubt on these results of angular distributions which were performed by using a direct spectrum.

2. Level scheme of ^{126}Te

The yrast excitations of ^{126}Te had been already studied up to $I^\pi = 10^+$ and 7^- from $^{124}\text{Sn}(\alpha, 2n)$ reaction [22]. Two new transitions were added in the positive-parity branch, leading to the (14^+) state, by means of deep inelastic $^{130}\text{Te} + ^{64}\text{Ni}$ reactions [4]. These two sets of states are confirmed in the present work. Moreover by using all the mutual $\gamma - \gamma - \gamma$ coincidences, we have extended the level scheme up to 6-MeV excitation energy, as shown in Fig. 2.

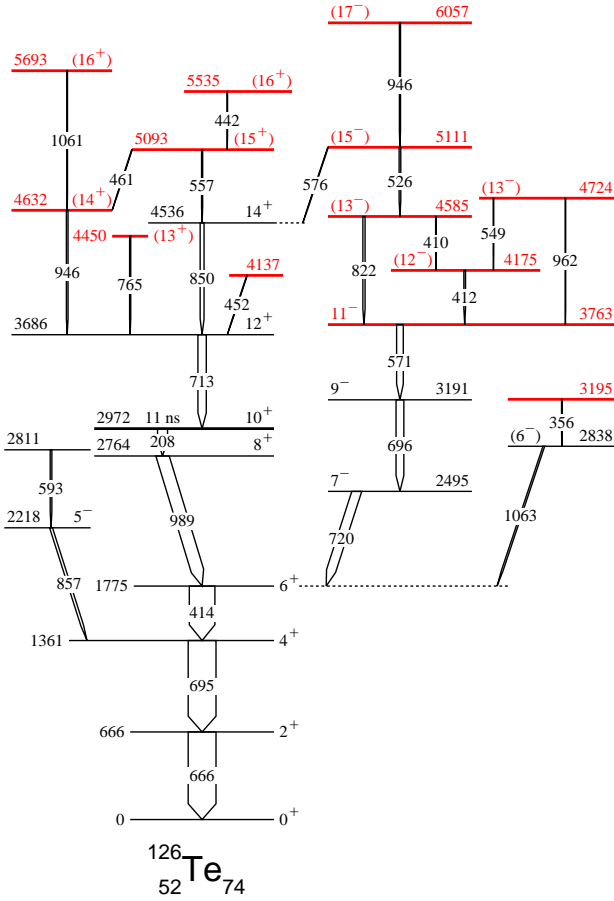


FIG. 2. (Color online) Level scheme of ^{126}Te deduced in the present work. The colored levels are new. The width of the arrows is proportional to the relative intensity of the γ rays. The half-life of the 2972-keV level is from Ref. [23].

Several new transitions which have been located above

the 7^- state form doublets with the low-lying γ rays. The 696.2-keV transition is close in energy with the $4^+ \rightarrow 2^+$ transition at 694.6 keV, and the 412.1- and 410.0-keV ones are close in energy with the $6^+ \rightarrow 4^+$ transition at 414.4 keV. The spectra given in Fig. 3 reveal these doublets. They show that 412- and 410-keV lines are detected in coincidence with the 414-keV one and that the 696-keV line is detected in coincidence with the 695-keV one.

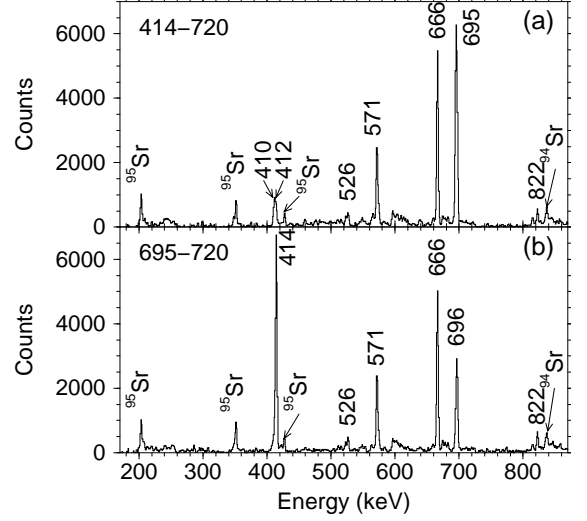


FIG. 3. Examples of coincidence spectra double-gated on two transitions of ^{126}Te , built from the $^{18}\text{O} + ^{208}\text{Pb}$ data set. The γ rays emitted by the Sr complementary fragments are labeled.

Angular correlations of successive γ rays have been extracted for the most intense transitions of ^{126}Te . The experimental results are given in Table II. The coincidence rates between the low-lying γ rays are in agreement with the results of the previous experiment [22] where the angular distributions were measured following the $^{124}\text{Sn}(\alpha, 2n)$ reaction. Moreover, the results given in Table II indicate that the 713-, 850-, 696-, and 571-keV transitions are quadrupole. Therefore the spin values of the 3686-, 4536-, 3191- and 3763-keV levels are 12^+ , 14^+ , 9^- , and 11^- , respectively. For the higher-spin part of the level scheme, we have assumed that the spin values increase with excitation energy and that the low-energy transitions have an $M1$ character.

We have gathered in Table III the properties of all the transitions assigned to ^{126}Te from this work.

A two-quasiparticle $K^\pi = 8^-$ isomeric state has been identified in many $N = 74$ isotones ($Z = 54 - 64$). Its excitation energy depends on the nuclear deformation, the minimum value (2233 keV) being observed for the most deformed isotone, ^{138}Gd [24]. Such a state has been predicted at 2980-keV excitation energy in ^{126}Te [25], which would exhibit shape coexistence as its ground state is quasi-spherical while the two quasineutrons leading to

TABLE II. Coincidence rates between the low-lying γ rays of ^{126}Te as a function of their relative angle of detection, normalized to the ones obtained around 75° .

$E_\gamma - E_\gamma$	$R(22^\circ)^{(a)}$	$R(46^\circ)^{(a)}$	$R(75^\circ)$
414 - 571	1.11(8)	1.04(5)	1.00
414 - 666	1.12(8)	1.06(5)	1.00
414 - 695/696	1.08(7)	1.05(5)	1.00
414 - 713	1.10(9)	1.03(5)	1.00
414 - 720	0.90(7)	0.95(5)	1.00
414 - 989	1.15(9)	1.08(6)	1.00
720 - 695/696	0.94(6)	0.98(5)	1.00
720 - 571	0.93(6)	0.98(5)	1.00
208 - 713	1.09(7)	1.03(6)	1.00
208 - 850	1.10(7)	1.03(6)	1.00

^(a) The number in parentheses is the error in the least significant digit shown.

TABLE III. Properties of the transitions assigned to ^{126}Te observed in this work.

$E_\gamma^{(a)}$ (keV)	$I_\gamma^{(a),(b)}$	$J_i^\pi \rightarrow J_f^\pi$	E_i	E_f
208.1(3)	35(7)	$10^+ \rightarrow 8^+$	2972.4	2764.3
356.5(5)	1.0(5)	$\rightarrow(6^-)$	3194.6	2838.1
410.0(5)	2(1)	$(13^-) \rightarrow (12^-)$	4584.9	4174.9
412.1(4)	5(2)	$(12^-) \rightarrow 11^-$	4174.9	3762.8
414.4(2)	92(14)	$6^+ \rightarrow 4^+$	1775.0	1360.6
442.4(5)	2.3(11)	$(16^+) \rightarrow (15^+)$	5535.5	5093.1
451.8(5)	1.8(9)	$\rightarrow 12^+$	4137.4	3685.6
461.0(5)	1.2(6)	$(15^+) \rightarrow (14^+)$	5093.1	4631.9
526.4(4)	4.9(15)	$(15^-) \rightarrow (13^-)$	5111.3	4584.9
549(1)	2(1)	$(13^-) \rightarrow (12^-)$	4724	4174.9
557.4(5)	2.8(14)	$(15^+) \rightarrow 14^+$	5093.1	4535.7
571.4(3)	23(5)	$11^- \rightarrow 9^-$	3762.8	3191.4
575.7(5)	1.5(7)	$(15^-) \rightarrow 14^+$	5111.3	4535.7
593(1)	5.0(2)	$\rightarrow 5^-$	2811	2218
666.0(2)	100	$2^+ \rightarrow 0^+$	666.0	0
694.6(3)	96(14)	$4^+ \rightarrow 2^+$	1360.6	666.0
696.2(3)	28(6)	$9^- \rightarrow 7^-$	3191.4	2495.2
713.2(3)	30(6)	$12^+ \rightarrow 10^+$	3685.6	2972.4
720.2(3)	34(7)	$7^- \rightarrow 6^+$	2495.2	1775.0
764.7(4)	4.2(17)	$(13^+) \rightarrow 12^+$	4450.3	3685.6
822.1(4)	7(2)	$(13^-) \rightarrow 11^-$	4584.9	3762.8
850.1(4)	13(3)	$14^+ \rightarrow 12^+$	4535.7	3685.6
857(1)	10(3)	$5^- \rightarrow 4^+$	2218	1360.6
945.8(5)	1.5(7)	$(17^-) \rightarrow (15^-)$	6057.1	5111.3
946.3(4)	5.5(16)	$(14^+) \rightarrow 12^+$	4631.9	3685.6
962(1)	1.6(8)	$(13^-) \rightarrow 11^-$	4724	3762.8
989.3(3)	45(9)	$8^+ \rightarrow 6^+$	2764.3	1775.0
1061.2(5)	1.3(6)	$(16^+) \rightarrow (14^+)$	5693.1	4631.9
1063.1(5)	5.1(15)	$(6^-) \rightarrow 6^+$	2838.1	1775.0

^(a) The number in parentheses is the error in the least significant digit shown.

^(b) The relative intensities are normalized to $I_\gamma(666) = 100$.

the $K^\pi = 8^-$ state drive the nucleus to a prolate shape ($\beta_2 = 0.12$). We have looked for isomeric states in ^{126}Te

by using the data registered with the SAPHIR detector. Only one γ -ray cascade has been found to be delayed, the one decaying the known 10^+ isomeric state (see Fig. 2). In conclusion, the $K^\pi = 8^-$ state of ^{126}Te could not be measured in our work, its energy is likely too large to allow for its population in the fusion-fission process. Moreover, because of its high excitation energy, the $K^\pi = 8^-$ state likely has a very short half-life, since it can decay to several excited states, such as the 7^- level at 2495 keV (see Fig. 2).

3. Level scheme of ^{128}Te

Several medium-spin states were known in ^{128}Te prior to this work. From the β decay of the $I^\pi = 8^-$ isomeric state of ^{128}Sb , yrast structures were unambiguously identified up to spin 6^+ and 7^- [26]. Later on, by using deep-inelastic reactions, a long-lived isomeric state was established by means of two delayed transitions populating the 6^+ level and assigned as the 10^+ level from the $(\nu h_{11/2})^2$ configuration [4]. Moreover four new γ rays were measured and located above the 10^+ state, spin and parity values of (12^+) and (14^+) being suggested for two of the newly-established levels.

All these yrast states are confirmed by the analyses of both data sets of the present work. Moreover, the spectra doubly-gated on the known transitions allowed us to identify many new γ lines which extend the level scheme up to 6.2 MeV excitation energy (see Fig. 4). Three parallel structures are found to populate the 3506-keV level. One of them is also linked to the 7^- state, defining the negative-parity band already known in the lighter isotopes. The two spectra shown in Fig. 5 display some of the new transitions belonging to these new structures.

Angular correlations of successive γ rays have been extracted for the most intense transitions of ^{128}Te . The experimental results are given in Table IV. The coincidence rates between the low-lying γ rays are in agreement with the results of the internal conversion electron measurements done in Ref. [26], following the β decay of ^{128}Sb , from which the spin and parity of the states located below 2.4-MeV excitation energy were determined. Moreover, the results given in Table IV indicate that the 387-, 563-, 629-, 717-, 813-, and 923-keV transitions have a stretched quadrupole character, while the 326-, 629-, 833-keV transitions have a stretched dipole one. Thus the spin and parity values of most of excited states in the energy range between 2.4 and 4.8 MeV are firmly assigned, such as the 12^+ and 14^+ states (see the left part of Fig. 4) and the 8^- , 9^- , 11^- , 13^- , 14^- , and 15^- states (see the right part of Fig. 4). In addition, the electric character of the 833-keV γ ray (which is a stretched-dipole transition from results of Table IV) is unambiguously determined from the fact that the $I = 13$ state is linked to the 7^- state by means of a cascade of three γ rays (two of them being stretched-quadrupole transitions). For the higher-spin part of the level scheme, we have assumed that the spin

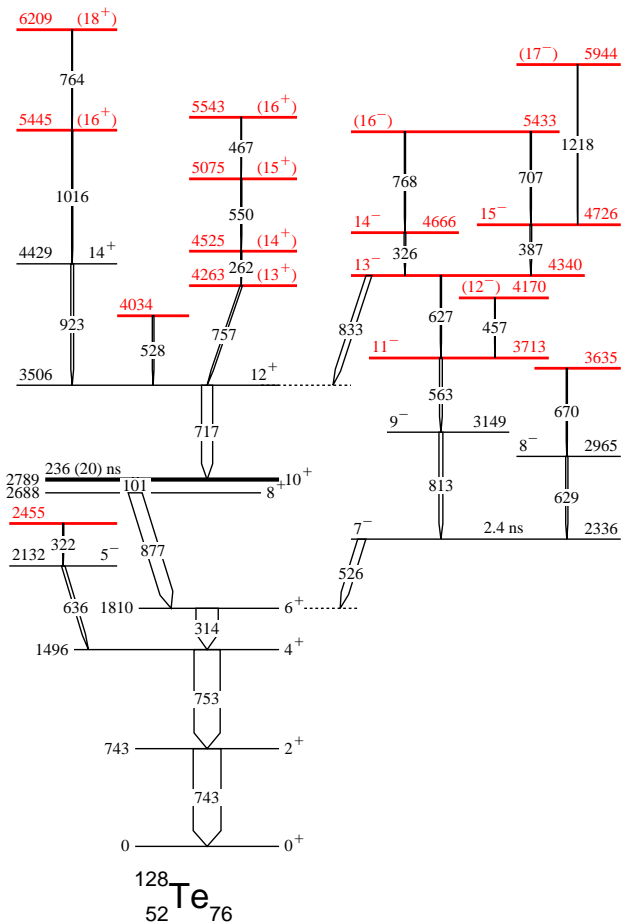


FIG. 4. (Color online) Level scheme of ^{128}Te deduced in the present work. The colored levels are new. The width of the arrows is proportional to the relative intensity of the γ rays. The half-life of the 2789-keV level is from this work and the one of the 2336-keV level is from Ref. [23].

values increases with excitation energy and that states close in excitation energy have the same spin value.

Noteworthy is the fact that the 14^+ yrast state is not the one previously proposed in Ref. [4]. There, the argument of the large intensity of the 833-keV transition was used to suggest that the 4340-keV level belongs to the positive-parity yrast band. Moreover the decay of the 3149-keV level, as well as the multipolarity of the 813-keV transition is at variance with that given in Ref. [26]. In that work, the 3149-keV level was firmly defined by the coincidence relationships of the intense 813-keV transition while two transitions having lower intensity were also proposed to deexcite this level, because their energies fit well the difference between the 3149-keV level and two low-lying levels. These two transitions (at 227 and 1340 keV) have not been observed in our gated spectra. In addition, the very low value of the K conversion coefficients given in Table 3 of Ref. [26] indicates that the 813-keV has an $E1$ character, while the results of the an-

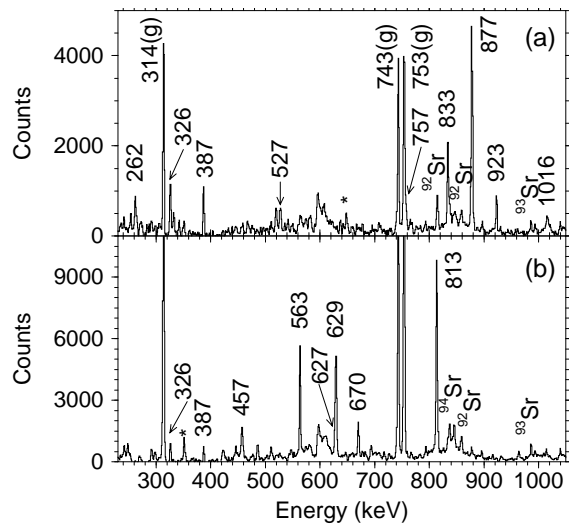


FIG. 5. Examples of coincidence spectra double-gated on two transitions of ^{128}Te , built from the $^{18}\text{O} + ^{208}\text{Pb}$ data set. The first gate is set on one of the first three yrast transitions and the second gate is set either on the 717-keV transition (a) or on the 526-keV transition (b). The γ rays emitted by the $^{92-94}\text{Sr}$ complementary fragments are labeled. The peaks marked with a star are contaminants.

TABLE IV. Coincidence rates between the low-lying γ -rays of ^{128}Te as a function of their relative angle of detection, normalized to the ones obtained around 75° .

$E_\gamma - E_\gamma$	$R(22^\circ)^{(a)}$	$R(46^\circ)^{(a)}$	$R(75^\circ)$
314 - 753	1.14(5)	1.07(5)	1.00
314 - 743	1.13(5)	1.06(5)	1.00
877 - 314	1.13(6)	1.04(6)	1.00
526 - 314	0.88(6)	0.97(6)	1.00
629 - 314	0.86(8)	0.92(7)	1.00
813 - 314	1.12(9)	1.05(5)	1.00
563 - 314	1.19(12)	1.10(8)	1.00
717 - 314	1.18(5)	1.06(5)	1.00
717 - 743	1.15(5)	1.10(5)	1.00
833 - 717	0.80(1)	0.90(5)	1.00
923 - 717	1.12(8)	1.08(7)	1.00
326 - 717	0.85(8)	0.95(6)	1.00
387 - 717	1.12(8)	1.05(5)	1.00

^(a) The number in parentheses is the error in the least significant digit shown.

gular correlation measurements done in the present work lead to an $E2$ one. Nevertheless, the value of the K conversion coefficient is questionable, as it does not seem to be in agreement with what can be seen in the conversion electron spectrum (see the figure 2 of Ref. [26]). Indeed the number of counts of the 813K line is very low, but it is of the same order as those of the 743L or 753L lines. Thus given the theoretical values of the L conversion coefficients (0.0003) and the relative intensity of the 813-keV transition (13%), one may compute the value of

the K conversion coefficient, $\alpha_K(813) \sim 0.002$, in good agreement with an $E2$ multipolarity.

As expected, the five γ rays deexciting the 10^+ isomeric state are observed in the SAPHIR experiment. The time distribution between the detection of two fragments by SAPHIR and the emission of one of the first four γ -rays of the yrast cascade (877-314-753-743) is shown in Fig. 6. In order to reduce the background, we have se-

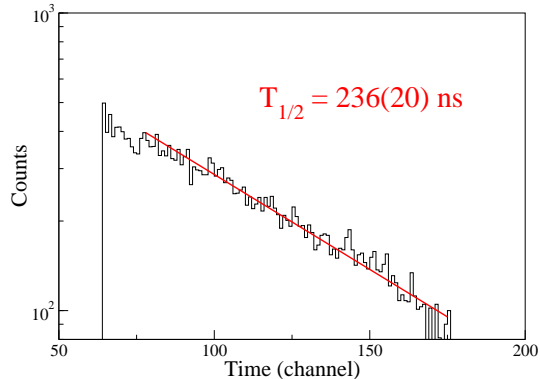


FIG. 6. (Color online) Half-life of the 2789 keV state of ^{128}Te obtained from the sum of the time distributions of the first four yrast transitions (743, 753, 314, and 877 keV). See text for further details about the procedures and the gating conditions.

lected the events containing a second γ -ray belonging to the cascade. The least-squares fit of this spectrum gives $T_{1/2} = 236(20)$ ns, a more precise value than that obtained from a previous analysis of the same data [27], $T_{1/2} = 250(40)$ ns. Thus the half-life of the 10^+ isomeric state of ^{128}Te is well shorter than that was reported in Ref. [4], $T_{1/2} = 0.37(3)\mu\text{s}$, and adopted in the last compilation [28]. The new value of the $B(E2; 10^+ \rightarrow 8^+)$, $85(7) e^2 fm^4$, i.e., $2.2(2)$ W.u., will be discussed below (see Sec. IV A 1).

We have gathered in Table V the properties of all the transitions assigned to ^{128}Te from this work.

4. Level scheme of ^{130}Te

The β decay of ^{130}Sb , similar to the one of ^{128}Sb , populates medium spin states of ^{130}Te . Its study led to the identification of the first yrast states of ^{130}Te , by means of γ -ray and conversion electron measurements [29]. Then, by using deep-inelastic reactions, a long-lived isomeric state ($T_{1/2} = 4.2(9)\mu\text{s}$) was proposed thanks to the observed delay of the first three yrast transitions as well as of two new γ lines, interpreted as the $8^+ \rightarrow 6^+$ and $8^+ \rightarrow 7^-$ transitions [4]. This isomeric state was assumed to be the expected 10^+ state from the $(\nu h_{11/2})^2$ configuration, the $10^+ \rightarrow 8^+$ transition being not detected because of its very low energy. Some years later, the conversion electrons of this transition was looked for,

TABLE V. Properties of the transitions assigned to ^{128}Te observed in this work.

$E_\gamma^{(a)}$ (keV)	$I_\gamma^{(a),(b)}$	$J_i^\pi \rightarrow J_f^\pi$	E_i	E_f
101.3(3)	17(4)	$10^+ \rightarrow 8^+$	2788.9	2687.6
262.1(4)	3.5(14)	$(14^+) \rightarrow (13^+)$	4525.2	4263.1
313.6(2)	80(12)	$6^+ \rightarrow 4^+$	1810.1	1496.5
322.4(5)	1.8(9)	$\rightarrow 5^-$	2454.9	2132.5
326.0(4)	6.2(19)	$14^- \rightarrow 13^-$	4665.6	4339.6
387.0(4)	5.4(22)	$15^- \rightarrow 13^-$	4726.6	4339.6
457.1(5)	2.8(14)	$(12^-) \rightarrow 11^-$	4169.7	3712.6
467.3(5)	1.0(5)	$(16^+) \rightarrow (15^+)$	5542.7	5075.4
526.3(3)	28(6)	$7^- \rightarrow 6^+$	2336.4	1810.1
527.6(4)	5.6(17)	$\rightarrow 12^+$	4033.6	3506.0
550.2(5)	1.6(8)	$(15^+) \rightarrow (14^+)$	5075.4	4525.2
563.1(4)	10(3)	$11^- \rightarrow 9^-$	3712.6	3149.5
627.1(5)	4.0(16)	$13^- \rightarrow 11^-$	4339.6	3712.6
629.2(4)	8(2)	$8^- \rightarrow 7^-$	2965.6	2336.4
636.0(4)	12(4)	$5^- \rightarrow 4^+$	2132.5	1496.5
670.1(4)	4.1(16)	$\rightarrow 8^-$	3635.7	2965.6
706.9(5)	2.9(14)	$(16^-) \rightarrow 15^-$	5433.4	4726.6
717.1(3)	40(8)	$12^+ \rightarrow 10^+$	3506.0	2788.9
743.0(2)	100	$2^+ \rightarrow 0^+$	743.0	0.0
753.5(2)	95(14)	$4^+ \rightarrow 2^+$	1496.5	743.0
757.1(4)	7(2)	$(13^+) \rightarrow 12^+$	4263.1	3506.0
764.1(7)	1.9(9)	$(18^+) \rightarrow (16^+)$	6209.2	5445.1
767.6(5)	4.8(19)	$(16^-) \rightarrow 14^-$	5433.4	4665.6
813.1(4)	15(4)	$9^- \rightarrow 7^-$	3149.5	2336.4
833.5(4)	18(4)	$13^- \rightarrow 12^+$	4339.6	3506.0
877.5(3)	48(10)	$8^+ \rightarrow 6^+$	2687.6	1810.1
922.6(4)	10(3)	$14^+ \rightarrow 12^+$	4428.6	3506.0
1016.5(5)	3.2(15)	$(16^+) \rightarrow 14^+$	5445.1	4428.6
1217.7(6)	1.8(9)	$(17^-) \rightarrow 15^-$	5944.3	4726.6

(a) The number in parentheses is the error in the least significant digit shown.

(b) The relative intensities are normalized to $I_\gamma(743) = 100$.

the ^{130}Te nuclei being produced by thermal neutron induced fission of Pu [30]. The $10^+ \rightarrow 8^+$ transition could not be observed, thus a conservative upper limit of its energy was proposed to be 25 keV. Nevertheless, by using the delayed γ rays, the half-life of the isomeric state was remeasured, $T_{1/2} = 1.90(8)\mu\text{s}$, i.e., more than a factor 2 smaller than the previous value.

High-spin states lying above 3-MeV excitation energy were identified from the observation of a new cascade of three delayed transitions, during the preliminary analysis of our SAPHIR experiment [31]. Later, the analysis of another deep-inelastic experiment, $^{136}\text{Xe} + ^{232}\text{Th}$, performed with the Gammasphere array [5] led to a more detailed decay of this new isomeric state. It displays new paths which allowed the authors of Ref. [5] to determine the energy of the long-lived 10^+ state, 18.5 keV above the 8^+ state. The new isomeric state was interpreted as the 15^- state arising from the maximum spin coupling of the four neutron holes, $(\nu h_{11/2})^{-3}(\nu d_{3/2})^{-1}$ [5]. It is worth pointing out that such a configuration has been recently established in neighboring even- A Sn isotopes,

where the 15^- state is also an isomeric state in the range of several tens to several hundreds of nanoseconds [6, 7].

All the yrast states of ^{130}Te previously identified have been observed in the present work. Moreover the careful analyses of the coincidence relationships allowed us to extend the level scheme by a few transitions (see Fig. 7).

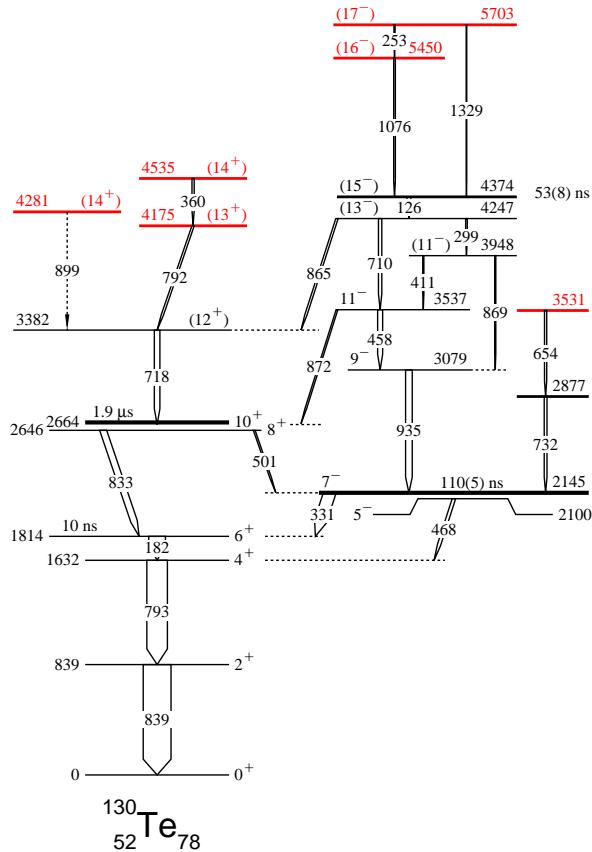


FIG. 7. (Color online) Level scheme of ^{130}Te deduced in the present work. The colored levels are new. The width of the arrows is proportional to the relative intensity of the γ rays. The half-lives of the 1814- and 2664-keV levels are from Ref. [23] and the ones of the 2145- and 4374-keV levels from this work.

Many values of spin and parity are unambiguously established, using both previous results on the electron conversion measurements [29] and present results on $\gamma - \gamma$ angular correlations. The K-conversion coefficients of the 182-, 793-, and 839-keV transitions lead to an $E2$ multipolarity, while that of the 331-keV transition corresponds to an $E1$ multipolarity. This is in good agreement with our results of angular correlations (see Table VI), which also give information on the 935- and 458-keV γ -rays, which have a quadrupole character. Thus the spin and parity values of all the yrast states are now determined up to $I = 11$. The spin and parity values proposed for the other states of the level scheme (see Fig. 7) are based on the arguments already used in the preceding sections.

TABLE VI. Coincidence rates between the low-lying γ rays of ^{130}Te as a function of their relative angle of detection, normalized to the ones obtained around 75° .

$E_\gamma - E_\gamma$	$R(22^\circ)^{(a)}$	$R(46^\circ)^{(a)}$	$R(75^\circ)$
182 - 793	1.10(7)	1.05(5)	1.00
182 - 839	1.09(7)	1.04(5)	1.00
331 - 182	0.89(8)	0.96(4)	1.00
331 - 839	0.89(7)	0.96(4)	1.00
935 - 839	1.11(8)	1.04(4)	1.00
935 - 331	0.88(7)	0.96(5)	1.00
458 - 331	0.85(9)	0.90(7)	1.00

(a) The number in parentheses is the error in the least significant digit shown.

As mentioned above, a high-energy isomeric state was measured in ^{130}Te [5, 31]. Its main decay path is illustrated by the spectrum of Fig. 8, which has been built from the data of SAPHIR experiment. The time distribution between the detection of two fragments by SAPHIR and the emission of one γ -ray of the 710-458-935 cascade is shown in Fig. 9. In order to reduce the background,

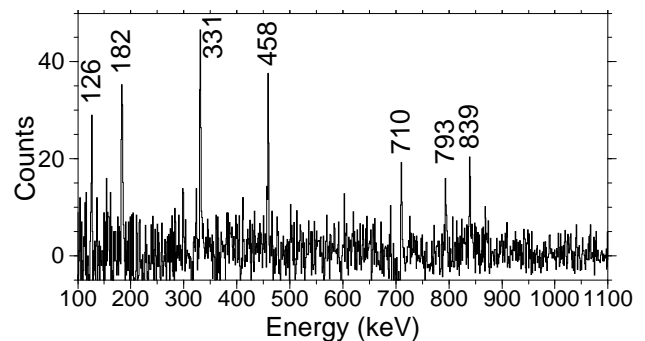


FIG. 8. Spectrum of γ -rays which are detected in the time interval 50 ns-1 μ s after the detection of two fragments by SAPHIR and in prompt coincidence with the 935-keV transition of ^{130}Te .

we have selected the events containing a second γ -ray belonging to the main decay path of the isomeric state, the 710-458-935-331-182-793-839 cascade. The fit of the time distribution gives $T_{1/2} = 53(8)\text{ns}$, which is in agreement with the value given in Ref. [5] within the error bars. In addition, we have computed the value of the total internal conversion coefficient of the 126-keV transition. Its intensity imbalance measured in spectra in double coincidence with one γ ray located above it and the other below it, leads to $\alpha_{tot}(126) = 0.7(2)$, in agreement with an $E2$ multipolarity, $\alpha_{tot}(126, E2, Z = 52) = 0.75$ [32]. Thus the $B(E2)$ value of the isomeric decay is $193(29) e^2 fm^4$, i.e., $4.9(7)$ W.u.. This value will be discussed in Sect. IV A 1.

For sake of completeness, we have remeasured the half-life of the 7^- state. For that purpose we did not use the data of the SAPHIR experiment since part of the population of the 7^- state comes from the decays of higher-lying

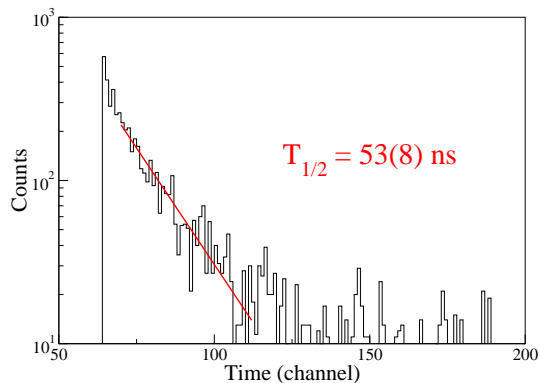


FIG. 9. (Color online) Half-life of the 4374 keV state of ^{130}Te obtained from the sum of the time distributions of the 935-, 458- and the 710-keV transitions. See text for further details about the procedures and the gating conditions.

isomeric states, mainly the 10^+ state with $T_{1/2} = 1.9 \mu\text{s}$. That gives rise to a second component in the time spectrum, which is not easy to subtract as the time window extends only to $1 \mu\text{s}$. Therefore we have used the timing information of the Ge detectors of Euroball (see Ref. [18] for the procedures and the calibrations). The time distribution between the emission of one transition populating the 7^- state (458- and 935-keV γ rays) and one transition involved in its decay (331- and 793-keV γ rays) is shown in Fig. 10. The slope, $T_{1/2} = 110(5)$ ns, is in good agreement with the previous value, 115(8) ns [29].

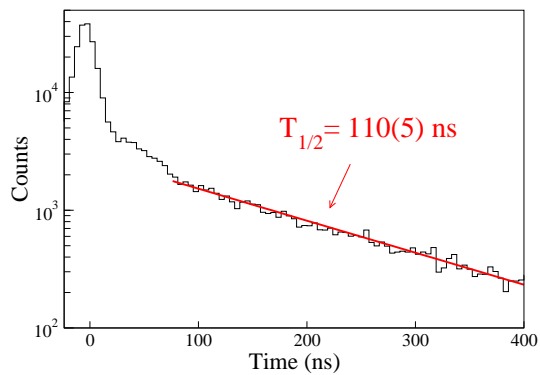


FIG. 10. (Color online) Time distribution between the emission of the 458- or 935-keV γ rays and of the 331- or 793-keV γ rays, built from the timing information of the Ge detectors. The slope is the half-life of the 2145-keV state of ^{130}Te .

We have gathered in Table VII the properties of all the transitions assigned to ^{130}Te from this work.

TABLE VII. Properties of the transitions assigned to ^{130}Te observed in this work.

$E_\gamma^{(a)}$ (keV)	$I_\gamma^{(a),(b)}$	$J_i^\pi \rightarrow J_f^\pi$	E_i	E_f
126.2(3)	14(4)	$(15^-) \rightarrow (13^-)$	4373.7	4247.5
181.8(3)	60(12)	$6^+ \rightarrow 4^+$	1814.2	1632.4
252.8(5)	4(2)	$(17^-) \rightarrow (16^-)$	5702.6	5449.7
299.0(5)	3(1)	$(13^-) \rightarrow (11^-)$	4247.5	3948.6
330.7(3)	43(11)	$7^- \rightarrow 6^+$	2144.9	1814.2
360.1(5)	4(2)	$(14^+) \rightarrow (13^+)$	4534.8	4174.7
411.4(5)	3(1)	$(11^-) \rightarrow 11^-$	3948.6	3537.4
458.0(4)	18(4)	$11^- \rightarrow 9^-$	3537.4	3079.4
467.9(4)	12(3)	$5^- \rightarrow 4^+$	2100.3	1632.4
501.5(5)	4.5(10)	$8^+ \rightarrow 7^-$	2646.4	2144.9
654.4(5)	8(3)		3531.0	2876.6
710.1(4)	13(4)	$(13^-) \rightarrow 11^-$	4247.5	3537.4
717.7(4)	19()	$(12^+) \rightarrow 10^+$	3382.2	2664.5
731.7(5)	9(3)	$\rightarrow 7^-$	2876.6	2144.9
792.5(5)	8(3)	$(13^+) \rightarrow (12^+)$	4174.7	3382.2
793.2(3)	74(15)	$4^+ \rightarrow 2^+$	1632.4	839.2
832.7(3)	25(5)	$8^+ \rightarrow 6^+$	2646.4	1814.2
839.2(3)	100	$2^+ \rightarrow 0^+$	839.2	0.0
865.2(5)	7(3)	$(13^-) \rightarrow (12^+)$	4247.5	3382.2
869.3(6)	2(1)	$(11^-) \rightarrow 9^-$	3948.6	3079.4
872.9(5)	6(2)	$11^- \rightarrow 10^+$	3537.4	2664.5
899(1)	2(1)	$(14^+) \rightarrow (12^+)$	4281.2	3382.2
934.5(4)	24(6)	$9^- \rightarrow 7^-$	3079.4	2144.9
1076.0(5)	6(2)	$(16^-) \rightarrow (15^-)$	5449.7	4373.7
1329.1(6)	2.5(12)	$(17^-) \rightarrow (15^-)$	5702.6	4373.7

^(a) The number in parentheses is the error in the least significant digit shown.

^(b) The relative intensities are normalized to $I_\gamma(839) = 100$.

B. Study of the odd- A $^{125-131}\text{Te}$ isotopes

1. Level scheme of ^{125}Te

Medium-spin states of ^{125}Te had been investigated using the $^{124}\text{Sn}(\alpha, 3n\gamma)$ reaction and in-beam techniques (excitation functions, $\gamma-\gamma$ coincidences and γ -ray angular distributions) [33]. This study led to the identification of three sets of levels, (i) three levels built on the $3/2_1^+$ state at 35.5 keV, (ii) three levels built on the $11/2_1^-$ state at 144.8 keV, (iii) two states decaying to both structures. Thus the level scheme extended up to 2.57 MeV excitation energy and a maximum spin value of $(23/2)$. Moreover some γ lines, assigned to ^{125}Te because of their excitation function, were not placed in the published level scheme.

The 601-555-378 triple coincidence is observed in our data set, meaning that the three levels built on the $3/2_1^+$ state at 35.5 keV [set (i)] are populated in the fusion-fission reactions. No other γ lines have been detected in coincidence with these three transitions, thus we do not confirm the existence of the 805- and 195-keV transitions which were placed above this structure because they fit the differences in energy between states established from coincidence relationships [33]. Hence the two highest-

spin states [set (iii)] only decay to the levels of set (ii).

Thanks to all the mutual $\gamma - \gamma - \gamma$ coincidences of our two data sets, we have extended the level scheme of ^{125}Te up to 5453-keV excitation energy (see Fig. 11). An example of doubly-gated coincidence spectra showing

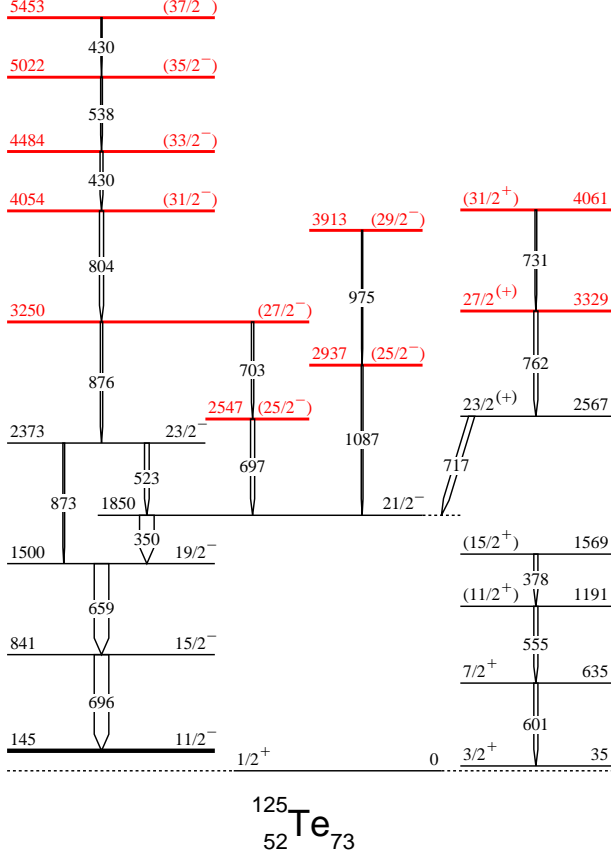


FIG. 11. (Color online) Level scheme of ^{125}Te deduced in the present work. The colored levels are new. The width of the arrows is proportional to the relative intensity of the γ rays. The energies of the $3/2^+$ state and of the isomeric $11/2^-$ state are from Ref. [23].

the transitions deexciting the new states of the left part of the level scheme is given in Fig. 12. This spectrum demonstrates that the 430-keV transition is a doublet, in self-coincidence. Moreover, our level scheme includes another doublet at 696 and 697 keV, the latter γ line being located between the 350- and the 703-keV transitions. Noteworthy is the fact that this doublet was not suspected in the previous work [33], thus the 703-keV transition was put in a wrong place.

The statistics of our ^{125}Te data being too low to perform $\gamma - \gamma$ angular correlation analyses, the spin assignments given in Fig. 11 come from the γ -ray angular distribution results of Ref. [33], namely, the 378-, 555-, 601-, 696-, 659-, 873- and 762-keV transitions are quadrupole ones with $\Delta I = 2$, and the 350-, 523- and 717-keV transitions are dipole ones with $\Delta I = 1$. That leads to the spin

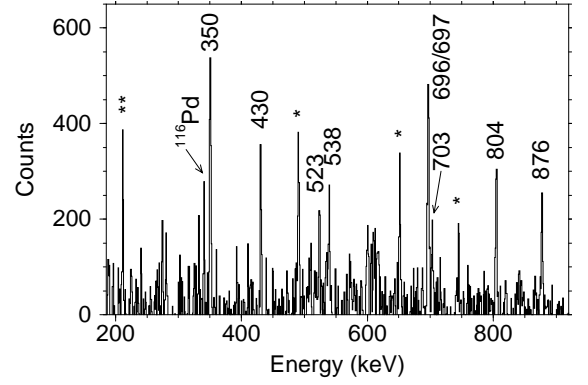


FIG. 12. (Color online) Coincidence spectrum double-gated on the 659- and 430-keV transitions of ^{125}Te , built from the $^{12}\text{C} + ^{238}\text{U}$ data set. The γ ray emitted by its main Pd complementary fragment is labeled. The peaks marked with a star are contaminants from ^{127}I , as its high-spin level scheme displays two transitions close in energy to those used to build the present spectrum (the transition emitted by its main Rh complementary fragment is marked with two stars).

and parity values given without parentheses in Fig. 11. The other values have been chosen by using the same arguments as in the preceding sections.

We have gathered in Table VIII the properties of all the transitions assigned to ^{125}Te from this work.

2. Level scheme of ^{127}Te

The β decay of ^{127}Sb was studied many years ago [23], leading to the identification of many states of ^{127}Te with an excitation energy below 1.4 MeV and I values around 7/2, which is the spin value of the ground state of ^{127}Sb . Among them, two states deserve to be quoted as they are expected to be populated in reactions induced by heavy ions, the $7/2^+$ state built on the $3/2^+$ ground state as well as the $11/2^-$ state from the promotion of the odd neutron to the $\nu h_{11/2}$ subshell. Indeed these two states were observed in deep-inelastic reactions, and new structures were proposed above them [4]. In this work, two new transitions were assigned to the structure built on the $3/2^+$ ground state and several states were discovered in the top of the structure built on the $11/2^-$ state.

Regarding the structure built on the $3/2^+$ ground state, we have not observed the 685-668-263 triple coincidence proposed in the latter work (see Table 2 of [4]). On the other hand, the 685-keV being detected in coincidence with transitions emitted by Sr fragments in the $^{18}\text{O} + ^{208}\text{Pb}$ reaction and by Pd fragments in the $^{12}\text{C} + ^{238}\text{U}$ reaction, we have looked for the other members of the cascade built on the $3/2^+$ ground state. As an example, the coincidence spectrum double-gated on the 685-keV transition of ^{125}Te and the 837-keV transition of ^{94}Sr , built from the $^{18}\text{O} + ^{208}\text{Pb}$ data set, shows two

TABLE VIII. Properties of the transitions assigned to ^{125}Te observed in this work. The energies of the $3/2_1^+$ state and of the isomeric $11/2^-$ state are from Ref. [23].

$E_\gamma^{(a)}$ (keV)	$I_\gamma^{(a),(b)}$	$J_i^\pi \rightarrow J_f^\pi$	E_i	E_f
349.9(3)	91(14)	$21/2^- \rightarrow 19/2^-$	1850.0	1500.1
377.7(4)	26(6)	$(15/2^+) \rightarrow (11/2^+)$	1568.5	1190.8
430.3(4)	10(3)	$(33/2^-) \rightarrow (31/2^-)$	4484.0	4053.7
430.3(5)	5(2)	$(37/2^-) \rightarrow (35/2^-)$	5452.7	5022.4
523.4(4)	27(5)	$23/2^- \rightarrow 21/2^-$	2373.4	1850.0
538.4(5)	7(2)	$(35/2^-) \rightarrow (33/2^-)$	5022.4	4484.0
554.7(4)	>26	$(11/2^+) \rightarrow 7/2^{+(c)}$	1190.8	636.1
600.6(4)	>26	$7/2^{+(c)} \rightarrow 3/2^+$	636.1	35.5
659.3(3)	>100	$19/2^- \rightarrow 15/2^-$	1500.1	840.8
696.0(3)	>100	$15/2^- \rightarrow 11/2^-$	840.8	144.8
696.8(4)	25(5)	$(25/2^-) \rightarrow 21/2^-$	2546.8	1850.0
702.7(4)	15(4)	$(27/2^-) \rightarrow (25/2^-)$	3249.7	2546.8
717.4(4)	34(7)	$23/2^{(+) } \rightarrow 21/2^-$	2567.4	1850.0
731.3(5)	9(3)	$(31/2^+) \rightarrow 27/2^{(+) }$	4060.6	3249.7
761.9(4)	27(5)	$27/2^{(+) } \rightarrow 23/2^{(+) }$	3329.3	2567.4
804.0(4)	14(3)	$(31/2^-) \rightarrow (27/2^-)$	4053.7	3680.0
873.2(5)	9(3)	$23/2^- \rightarrow 19/2^-$	2373.4	1500.1
876.4(4)	14(4)	$(27/2^-) \rightarrow 23/2^-$	3249.7	2373.4
975.3(5)	6(2)	$(29/2^-) \rightarrow (25/2^-)$	3912.6	2937.3
1087.3(5)	8(3)	$(25/2^-) \rightarrow 21/2^-$	2937.3	1850.0

(a) The number in parentheses is the error in the least significant digit shown.

(b) The relative intensities are normalized to the sum of the populations of the $19/2^-$ state, $I_\gamma(350) + I_\gamma(873) = 100$.

(c) Spin value from Ref. [34].

new transitions at 604 and 381 keV [see Fig 13(a)], which do not belong to ^{94}Sr . Second, the coincidence spectrum double-gated on the 685- and 604-keV transition of ^{125}Te confirms the existence of the 381-keV γ line, as well as the correlation of all the Sr complementary fragments. Similar results are obtained by using the $^{12}\text{C} + ^{238}\text{U}$ data set, the 685-604-381 triple coincidence of ^{127}Te and the correlation to the transitions emitted by the Pd complementary fragments.

All the states belonging to the structure built on the $11/2^-$ state [4] have been confirmed by the analyses of both data sets of the present work. In total, nine new states have been identified at higher energy, extending the level scheme up to 4.82 MeV excitation energy (see Fig. 14).

Angular correlations of successive γ rays have been extracted for the most intense transitions of ^{127}Te . The experimental results are given in Table IX. They show that the 697-, 678-, 953-keV transitions, as well as the 591- and 816-keV ones, are quadrupole, while the 358-, 392-, 458-, and 491-keV transitions are dipole. This defines the spin values of several excited states, which are given in Fig. 14. The spin assignments of the higher-lying states, given in parentheses, are based on the same arguments as those used in the preceding sections.

We have gathered in Table X the properties of all the

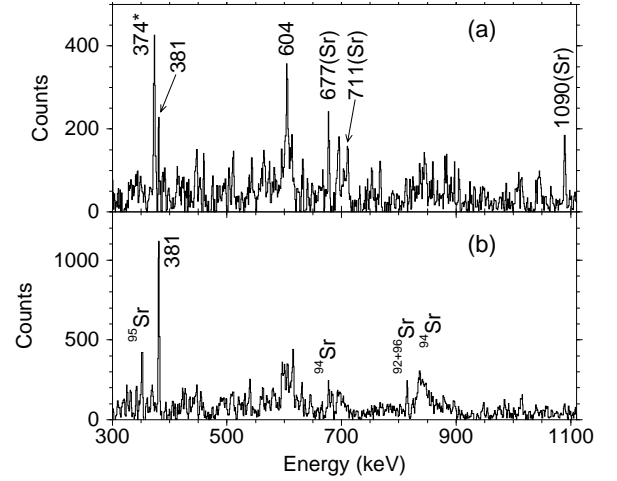


FIG. 13. (a) Coincidence spectrum double-gated on the 685-keV transition of ^{127}Te and the 837-keV transition of ^{94}Sr , built from the $^{18}\text{O} + ^{208}\text{Pb}$ data set. The γ rays known to be emitted by ^{94}Sr are labeled by Sr. The peak at 374 keV marked with a star is a contaminant belonging to ^{110}Pd , where the 374-838-688 triple coincidence occurs. (b) Coincidence spectrum double-gated on the 685- and 604-keV transition of ^{125}Te , the γ rays emitted by its Sr complementary fragments are labeled.

TABLE IX. Coincidence rates between the low-lying γ rays of ^{127}Te as a function of their relative angle of detection, normalized to the ones obtained around 75° .

$E_\gamma - E_\gamma$	$R(22^\circ)^{(a)}$	$R(46^\circ)^{(a)}$	$R(75^\circ)$
358 - 491	1.06(4)	1.05(4)	1.00
358 - 678	0.95(4)	0.96(4)	1.00
392 - 458	1.08(4)	1.03(3)	1.00
392 - 678	0.80(5)	0.94(4)	1.00
392 - 697	0.80(4)	0.95(4)	1.00
678 - 458	0.95(4)	0.95(4)	1.00
678 - 591	1.14(5)	1.04(4)	1.00
678 - 953	1.14(5)	1.07(3)	1.00
816 - 392	0.90(5)	0.95(5)	1.00
816 - 458	0.93(3)	0.96(4)	1.00
816 - 697	1.2(1)	1.07(6)	1.00
953 - 591	1.11(5)	1.07(4)	1.00

(a) The number in parentheses is the error in the least significant digit shown.

transitions assigned to ^{127}Te from this work.

3. Level scheme of ^{129}Te

The first results on the excited states of ^{129}Te were obtained from the β -decay studies of ^{129}Sb , in which an iso-

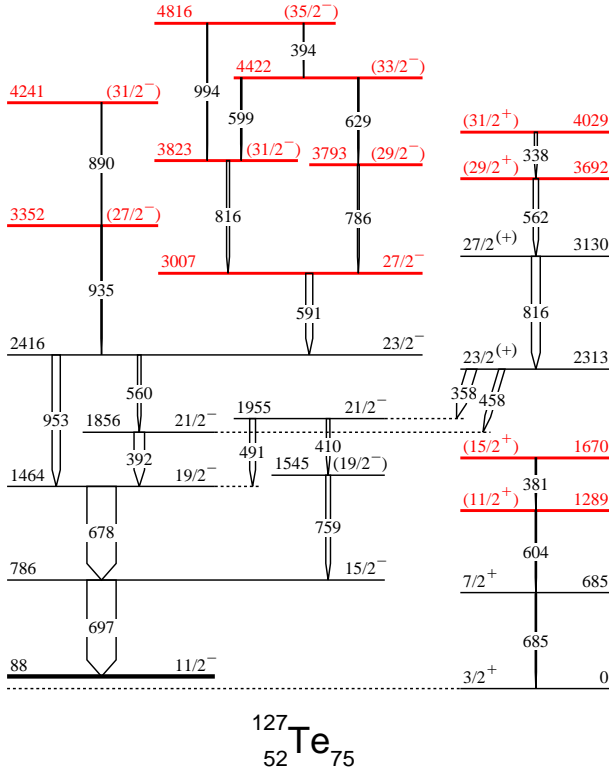


FIG. 14. (Color online) Level scheme of ^{127}Te deduced in the present work. The colored levels are new. The width of the arrows is proportional to the relative intensity of the γ rays. The energy of the long-lived isomeric $11/2^-$ state is from Ref. [23].

meric state was discovered many years ago [36]. Several years later, its spin value, $I^\pi = 19/2^-$, was established thanks to the $M4$ internal transition [37]. Given that the β branching of the $^{129}\text{Sb}^m$ decay is 85%, several high-spin states of ^{129}Te populated by this decay were finally unambiguously identified by using results of another measurement, in which the ^{129}Te nuclei were produced in deep-inelastic $^{130}\text{Te} + ^{64}\text{Ni}$ reactions [38]. Then the high-spin level scheme of ^{129}Te was defined up to 2.1 MeV excitation energy and spin value of $23/2^+$. Later on, a more detailed analysis of the deep-inelastic measurements led to assign two new transitions, which extended the level scheme to 3 MeV excitation energy [4].

All the yrast states of ^{129}Te have been confirmed by the analyses of both data sets of the present work. Moreover the spectra doubly-gated on the known transitions allowed us to identify many new γ lines which extend the level scheme up to 4.825 MeV. For instance, the spectrum of Fig. 15 shows the new transitions located above the 2136-keV state.

The level scheme built from these analyses is shown

TABLE X. Properties of the transitions assigned to ^{127}Te observed in this work. The energy of the isomeric $11/2^-$ state is from Ref. [23].

$E_\gamma^{(a)}$ (keV)	$I_\gamma^{(a),(b)}$	$J_i^\pi \rightarrow J_f^\pi$	E_i	E_f
337.8(3)	9(3)	$(31/2^+) \rightarrow (29/2^+)$	4029.7	3691.9
358.2(3)	30(6)	$23/2^{(+)} \rightarrow 21/2^-$	2313.2	1954.9
381.0(5)	4(2)	$(15/2^+) \rightarrow (11/2^+)$	1669.8	1288.8
392.0(3)	31(6)	$21/2^- \rightarrow 19/2^-$	1855.7	1463.7
394.1(5)	2(1)	$(35/2^-) \rightarrow (33/2^-)$	4816.1	4422.1
410.3(3)	10(3)	$21/2^- \rightarrow (19/2^-)$	1954.9	1544.6
457.6(3)	18(4)	$23/2^{(+)} \rightarrow 21/2^-$	2313.2	1855.7
491.3(3)	17(4)	$21/2^- \rightarrow 19/2^-$	1954.9	1463.7
560.5(3)	10(3)	$23/2^- \rightarrow 21/2^-$	2416.3	1855.7
562.3(3)	15(4)	$(29/2^+) \rightarrow 27/2^{(+)}$	3691.9	3129.6
590.6(3)	20(5)	$27/2^- \rightarrow 23/2^-$	3006.9	2416.3
599.2(5)	3.6(14)	$(33/2^-) \rightarrow (31/2^-)$	4422.0	3822.6
604.2(6)	>4	$(11/2^+) \rightarrow 7/2^{(c)}$	1288.8	684.6
629.4(6)	2.8(14)	$(33/2^-) \rightarrow (29/2^-)$	4422.0	3792.7
678.1(2)	87(13)	$19/2^- \rightarrow 15/2^-$	1463.7	785.6
684.6(6)	>4	$7/2^{(c)} \rightarrow 3/2^+$	684.6	0
697.4(2)	>100	$15/2^- \rightarrow 11/2^-$	785.6	88.2
759.0(4)	13(3)	$(19/2^-) \rightarrow 15/2^-$	1544.6	785.6
785.8(5)	5.7(17)	$(29/2^-) \rightarrow 27/2^-$	3792.7	3006.9
815.7(5)	8(3)	$(31/2^-) \rightarrow 27/2^-$	3822.6	3006.9
816.4(4)	25(5)	$27/2^{(+)} \rightarrow 23/2^{(+)}$	3129.6	2313.3
889.3(7)	1.0(5)	$(31/2^-) \rightarrow (27/2^-)$	4240.9	3351.6
935.2(6)	3.2(15)	$(27/2^-) \rightarrow 23/2^-$	3351.6	2416.3
952.7(4)	24(5)	$23/2^- \rightarrow 19/2^-$	2416.3	1463.7
993.8(7)	1.4(7)	$(35/2^-) \rightarrow (31/2^-)$	4816.1	3822.6

- (a) The number in parentheses is the error in the least significant digit shown.
(b) The relative intensities are normalized to the sum of the populations of the $15/2^-$ state, $I_\gamma(678) + I_\gamma(759) = 100$.
(c) Spin value from Ref. [35].

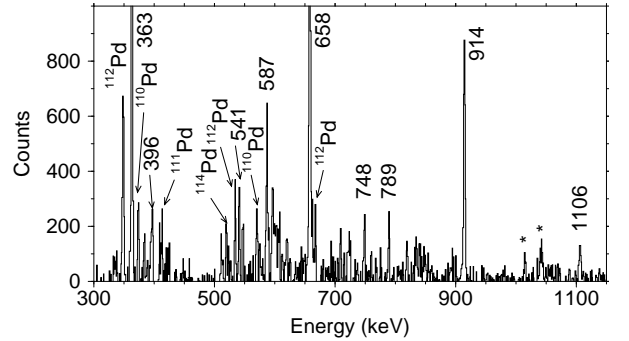


FIG. 15. Coincidence spectrum double-gated on the 759- and 251-keV transitions of ^{129}Te , built from the $^{12}\text{C} + ^{238}\text{U}$ data set. The γ rays emitted by its main Pd complementary fragments are labeled. The peaks marked with a star are identified contaminants.

in Fig. 16. Its high-energy part comprises two independent structures, one built on the 2136-keV state and the other on the 2510-keV state, which have different pari-

ties according to the previous work [4]. In addition the

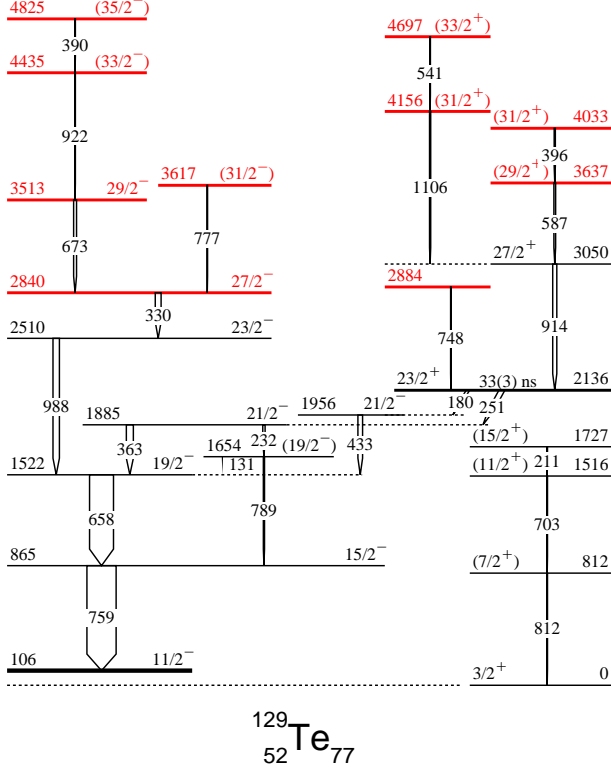


FIG. 16. (Color online) Level scheme of ^{129}Te deduced in the present work. The colored levels are new. The width of the arrows is proportional to the relative intensity of the γ rays. The energy of the long-lived isomeric $11/2^-$ state is from Ref. [23] and the half-life of the 2136-keV isomeric state from Ref. [38].

triple coincidence, 812-703-211, proposed in the previous work, which defines the structure built on the $3/2^+$ ground state, is observed in both data sets of the present work. Even though the number of counts associated to these γ lines is too low to observe their coincidences with the transitions emitted by the complementary fragments, we adopt the same assignment as previously (see Fig. 16).

Angular correlations of successive γ rays have been extracted for the most intense transitions of ^{129}Te . The experimental results are given in Table XI. They show that five transitions have a quadrupole character, the 759-, 658-, 988-, 330-keV transitions located in the left side of the level scheme (see Fig. 16) and the 914-keV one located in the right side. In addition, the four transitions linking the two parts (at 180, 251, 363 and 433 keV) are dipole. Then the spin values of most of the states located below 3513-keV excitation energy are now determined. A positive parity is assigned to the 2136-keV state because of its delayed decay, which can be explained only if the dipole 180- and 251-keV γ rays are $E1$ [38]. The values of the reduced transition probabilities (given in Table XVII) will be discussed in Sect. IV A 2. The spin values given

TABLE XI. Coincidence rates between the low-lying γ rays of ^{129}Te as a function of their relative angle of detection, normalized to the ones obtained around 75° .

$E_\gamma - E_\gamma$	$R(22^\circ)^{(a)}$	$R(46^\circ)^{(a)}$	$R(75^\circ)$
759 - 330	1.10(5)	1.06(3)	1.00
759 - 433	0.87(8)	0.96(4)	1.00
759 - 673	0.8(1)	0.90(7)	1.00
759 - 914	1.17(8)	1.08(4)	1.00
759 - 988	1.12(6)	1.04(3)	1.00
914 - 180	0.91(5)	0.95(5)	1.00
914 - 251	0.92(6)	0.89(8)	1.00
914 - 363	0.8(1)	0.92(6)	1.00
914 - 658	1.16(8)	1.05(4)	1.00
988 - 330	1.15(9)	1.07(5)	1.00

(a) The number in parentheses is the error in the least significant digit shown.

in parentheses have been chosen by using the same arguments as in the preceding sections.

We have gathered in Table XII the properties of all the transitions assigned to ^{129}Te from this work.

TABLE XII. Properties of the transitions assigned to ^{129}Te observed in this work. The energy of the isomeric $11/2^-$ state is from Ref. [23].

$E_\gamma^{(a)}$ (keV)	$I_\gamma^{(a),(b)}$	$J_i^\pi \rightarrow J_f^\pi$	E_i	E_f
130.9(5)	4(2)	$(19/2^-) \rightarrow 19/2^-$	1653.5	1522.4
180.1(4)	9.4(28)	$23/2^+ \rightarrow 21/2^-$	2135.8	1955.8
211.4(5)	1.4(7)	$(15/2^+) \rightarrow (11/2^+)$	1727.1	1515.7
231.6(3)	8(2)	$21/2^- \rightarrow (19/2^-)$	1885.2	1653.5
250.5(3)	17(4)	$23/2^+ \rightarrow 21/2^-$	2135.8	1885.2
330.4(3)	19(5)	$27/2^- \rightarrow 23/2^-$	2840.3	2509.9
362.9(3)	23(5)	$21/2^- \rightarrow 19/2^-$	1885.2	1522.4
389.9(5)	1.4(7)	$(35/2^-) \rightarrow (33/2^-)$	4825.1	4435.3
396.4(5)	2.7(13)	$(31/2^+) \rightarrow (29/2^+)$	4033.0	3636.6
433.4(3)	16(4)	$21/2^- \rightarrow 19/2^-$	1955.8	1522.4
541.2(5)	2(1)	$(33/2^+) \rightarrow (31/2^+)$	4696.7	4155.5
586.8(4)	6.4(19)	$(29/2^+) \rightarrow 27/2^+$	3636.6	3049.8
657.5(2)	82(12)	$19/2^- \rightarrow 15/2^-$	1522.4	864.9
672.6(4)	10(3)	$29/2^- \rightarrow 27/2^-$	3512.9	2840.3
703.3(6)	>1.4	$(11/2^+) \rightarrow (7/2^+)^{(c)}$	1515.7	812.4
748.0(6)	1.8(9)	$\rightarrow 23/2^+$	2883.8	2135.8
759.4(2)	100	$15/2^- \rightarrow 11/2^-$	864.9	105.5
776.7(6)	2(1)	$(31/2^-) \rightarrow 27/2^-$	3617.0	2840.3
788.8(6)	5(2)	$(19/2^-) \rightarrow 15/2^-$	1653.5	864.9
812.4(6)	>1.4	$(7/2^+)^{(c)} \rightarrow 3/2^+$	812.4	0.0
914.1(4)	13(3)	$27/2^+ \rightarrow 23/2^+$	3049.8	2135.8
922.4(6)	2(1)	$(33/2^-) \rightarrow 29/2^-$	4435.3	3512.9
987.5(4)	22(4)	$23/2^- \rightarrow 19/2^-$	2509.9	1522.4
1105.7(6)	3.0(12)	$(31/2^+) \rightarrow 27/2^+$	4155.5	3049.8

(a) The number in parentheses is the error in the least significant digit shown.

(b) The relative intensities are normalized to $I_\gamma(759) = 100$.

(c) Spin value from Ref. [39].

4. Level scheme of ^{131}Te

Very few high-spin levels were known in ^{131}Te prior to this work. In a first experiment, three transitions (at 833, 565 and 361 keV) were identified from deep inelastic $^{130}\text{Te} + ^{64}\text{Ni}$ reactions [4] and assigned, on the basis of systematics, as the $21/2^- \rightarrow 19/2^- \rightarrow 15/2^- \rightarrow 11/2^-$ cascade. Since these transitions were observed to decay slowly in the off-beam spectra ($T_{1/2} > 1\mu\text{s}$), the authors assumed that the $23/2^+$ state lies just above the $21/2^-$ state and decays by a low-energy transition which is delayed. In a second experiment performed at the Osiris mass separator, a very long-lived isomeric state of ^{131}Te ($T_{1/2} = 93\text{ ms}$) was discovered following the thermal fission of U isotopes and identified as the expected $23/2^+$ state [40]. The same three transitions were observed for its decay. In addition, the conversion electron measurements showed that the 361-keV transition, having a high multipolarity, is the delayed transition. On the basis of the values of the reduced transition probabilities, the authors of Ref. [40] chose the $E3$ multipolarity. But it is worth mentioning that $M2$ and $E3$ multiplicities lead to similar values of α_K coefficient in this case, so an $M2$ character for the 361-keV transition has not to be excluded when only considering the experimental results.

The 833-564-361 triple coincidence has been also observed in the two data sets of the present work. No other transition is correlated to this cascade, in agreement with the decay of an isomeric state, as proposed in the previous works. Moreover, since none of these γ lines are measured in the SAPHIR experiment, the half-life has to be well longer than $10\mu\text{s}$.

On the other hand, the spectrum double-gated on the two first transitions exhibits new transitions which do not belong to the complementary fragments. Two examples of coincidence spectra double-gated on new transitions of ^{131}Te are shown in Fig. 17. So a cascade of five new transitions is unambiguously assigned to ^{131}Te , extending the structure built on the $11/2^-$ state up to 4688 keV (see Fig. 18).

Angular correlation measurements could not be performed, since the statistics of the ^{131}Te γ rays is too low. Thus the spin and parity values (given in parentheses in Fig. 18) have been chosen by analogy with the level structures of the lighter isotopes. The 1016- and 1580-keV states are assumed to be the $15/2^-$ and $19/2^-$ levels, respectively and the long-lived isomeric state, the $23/2^+$ level. Thus the 361-keV transition has an $M2$ character, at variance with the choice made by the authors of Ref. [40]. The very low value of the reduced transition probability of the isomeric transition, $B(M2; 23/2^+ \rightarrow 19/2^-) = 2 \times 10^{-6}$ W.u., will be discussed in Sect. IV A 2.

We have gathered in Table XIII the properties of all the transitions assigned to ^{131}Te from this work.

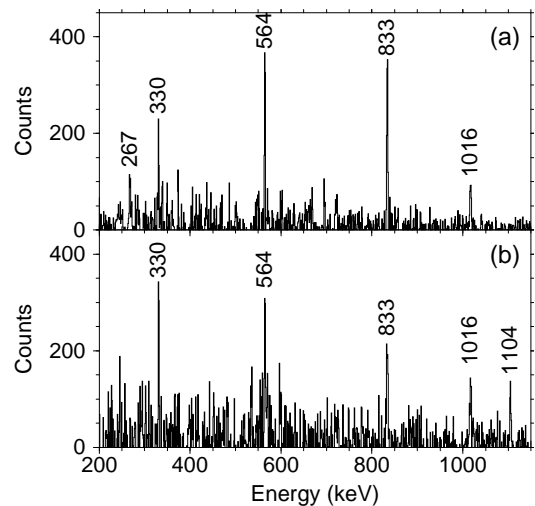


FIG. 17. Coincidence spectra double-gated on new transitions of ^{131}Te , built from the $^{12}\text{C} + ^{238}\text{U}$ data set. (a) the gates are set on the 391- and 1104-keV transitions, (b) the gates are set on the 267- and 391-keV transitions.

TABLE XIII. Properties of the transitions assigned to ^{131}Te observed in this work. The energy of the isomeric $11/2^-$ state is from Ref. [23].

$E_\gamma^{(a)}$ (keV)	$I_\gamma^{(a),(b)}$	$2J_i^\pi \rightarrow 2J_f^\pi$	E_i	E_f
266.7(5)	7(3)	$(35^-) \rightarrow (33^-)$	4688.0	4421.3
330.2(5)	12(5)	$(33^-) \rightarrow (29^-, 31^-)$	4421.3	4091.1
361(1)	18(6)	$(23^+) \rightarrow (19^-)$	1941	1579.9
390.7(5)	25(5)	$(27^-) \rightarrow (23^-)$	3074.8	2684.1
564.3(4)	100	$(19^-) \rightarrow (15^-)$	1579.9	1015.6
833.3(4)	>100	$(15^-) \rightarrow 11^-$	1015.6	182.3
1016.3(5)	17(6)	$(29^-, 31^-) \rightarrow (27^-)$	4091.1	3074.8
1104.2(5)	36(9)	$(23^-) \rightarrow (19^-)$	2684.1	1579.9

(a) The number in parentheses is the error in the least significant digit shown.

(b) The relative intensities are normalized to $I_\gamma(564) = 100$.

C. $^{132-136}\text{Te}$ and observation of several singular partners

As mentioned in the introduction of Sect. III, ^{132}Te is located in the high- A tail of the Te fragment distribution in both fusion-fission reactions used in the present work. Thus the γ rays emitted by its first excited states are barely observed and we could not find any new cascade to be placed above its two long-lived isomeric states, $I^\pi = 7^-$ and 10^+ [30].

However, in the C+U reaction, we have also identified γ rays emitted by four other isotopes with heavier masses, $^{133-136}\text{Te}$. The transitions deexciting the $I^\pi = 19/2^-$ isomeric states of ^{133}Te and ^{135}Te , as well as those of the $I^\pi = 6^+$ isomeric state of ^{134}Te are clearly observed in the SAPHIR experiment. Moreover, several γ lines known to be located in the medium-spin part of the $^{134,136}\text{Te}$

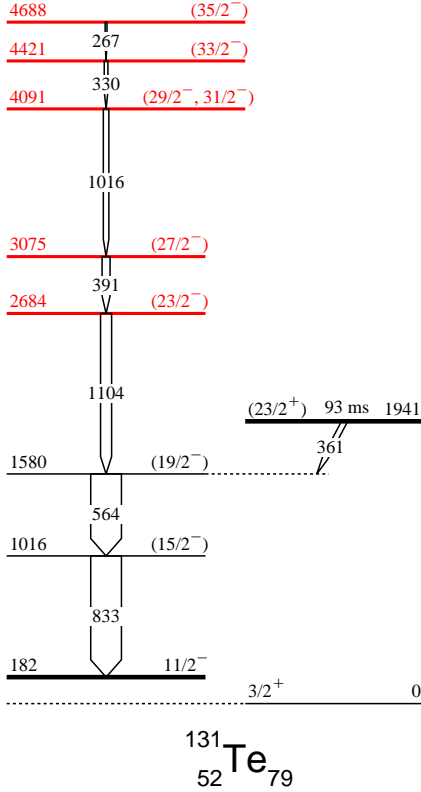


FIG. 18. (Color online) Level scheme of ^{131}Te deduced in the present work. The colored levels are new. The width of the arrows is proportional to the relative intensity of the γ rays. The energy of the long-lived isomeric $11/2^-$ state is from Ref. [23] and the half-life of the 1941-keV isomeric state from Ref. [40].

level schemes [41, 42] are seen in the spectrum gated by their two first transitions, in the Euroball experiment (see, for instance, the spectrum of Fig. 19). In addition, γ rays emitted by $^{102,104}\text{Mo}$ are unambiguously observed in the doubly-gated spectrum of ^{134}Te (five transitions are labeled in Fig. 19). In this case, the total number of protons of the two partners is 94, instead of $Z_{tot} = 98$ obtained for $^{124-130}\text{Te}$ which are produced from the C+U complete fusion.

The spectra doubly-gated by the first transitions of many neighboring fission fragments were then carefully analyzed in order to know whether a total number of protons lower than 98 is obtained for other couples of partners. The results are gathered in Table XIV.

While the γ rays of $^{128-136}_{54}\text{Xe}$ isotopes are only detected in coincidence with those of ^{44}Ru , the partners of ^{138}Xe are numerous, Zr, Mo and Ru. This shows that the fissioning nuclei are ^{94}Pu , ^{96}Cm and ^{98}Cf , respectively. Similar results are found for several heavy ^{56}Ba and ^{58}Ce isotopes.

In summary, many heavy- A fragments, belonging to the region located just above ^{132}Sn , come from the fis-

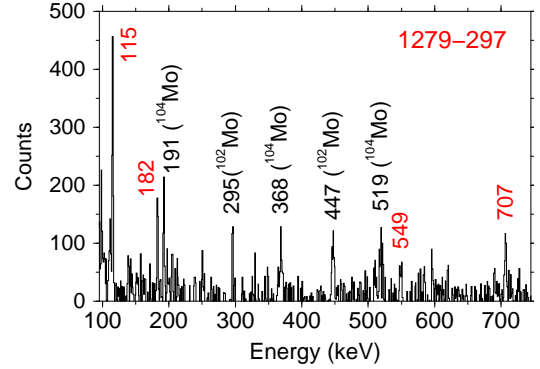


FIG. 19. (Color online) Coincidence spectrum double-gated on the two first transitions of ^{134}Te , built from the $^{12}\text{C} + ^{238}\text{U}$ data set. The γ rays emitted by ^{134}Te are written in red and those by the ^{42}Mo complementary fragments in black.

TABLE XIV. List of singular partners observed in the $^{12}\text{C} + ^{238}\text{U}$ reaction.

fragment	partners set 1	partners set 2	partners set 3
^{146}Ce	$^{94-97}\text{Zr}$	^{94}Sr	
^{144}Ce	$^{94-97}\text{Zr}$	^{94}Sr	
^{144}Ba	^{98}Mo		^{94}Sr
^{142}Ba	$^{100-102}\text{Mo}$	$^{96-98}\text{Zr}$	^{96}Sr
^{140}Xe			^{98}Zr
^{138}Xe	^{104}Ru	^{102}Mo	$^{98-100}\text{Zr}$
^{134}Te			$^{102,104}\text{Mo}$
$A_a + A_b$	240-244	238-240	236-238
$Z_a + Z_b$	98	96	94

sion of Pu and Cm isotopes. The Pu and Cm nuclei are produced in particular exit channels of the C+U reaction, $^{238}\text{U} (^{12}\text{C}, ^8\text{Be}) ^{242}\text{Pu}^*$ and $^{238}\text{U} (^{12}\text{C}, ^4\text{He}) ^{246}\text{Cm}^*$, i.e., incomplete fusion or transfer reactions. Thanks to the identification of their partners, the production of the most neutron-rich Te, Xe, and Ba isotopes is unambiguously attributed to the fission of Pu isotopes and thus cannot be misinterpreted by the existence of particular shell effects which would be at work in the low-energy fission of Cf isotopes, produced in the C+U complete fusion at 90-MeV bombarding energy.

IV. DISCUSSION

A. General features of the high-spin structures of the heavy Te isotopes

The high-spin structures of the heavy Te isotopes are expected to be more intricate than the ones of the Sn isotopes since, in addition to the breaking of neutron pairs

observed in Sn isotopes [6–8], the breaking of the proton pair has to be taken into account. Table XV gives the various configurations expected in the heavy- A Te isotopes when the valence space includes the $\nu h_{11/2}$ and $\nu d_{3/2}$ subshells, as well as the $\pi g_{7/2}$ and $\pi d_{5/2}$ ones. Noteworthy is the fact that the increase of the angular momentum within the yrast line would involve alternatively or simultaneously the neutron-pair and the proton-pair breakings.

TABLE XV. Various configurations expected in heavy- A Te isotopes with several broken pairs belonging to the subshells close to the Fermi levels ($\nu h_{11/2}$, $\nu d_{3/2}$, $\pi g_{7/2}$, and $\pi d_{5/2}$). The seniority, S , of each configuration is given in the fourth column. The I_{max}^π value corresponding to the breaking of one $\nu h_{11/2}$ pair is written in bold.

Neutron part	Proton part	I_{max}^π	S
	$(\pi g_{7/2})^2$ or $(\pi g_{7/2})^1(\pi d_{5/2})^1$	6^+	2
$(\nu h_{11/2})^2$		10^+	2
$(\nu h_{11/2})^2$	$(\pi g_{7/2})^2$ or $(\pi g_{7/2})^1(\pi d_{5/2})^1$	16^+	4
$(\nu h_{11/2})^4$		16^+	4
$(\nu h_{11/2})^6$		18^+	6
$(\nu h_{11/2})^1(\nu d_{3/2})^1$		7^-	2
$(\nu h_{11/2})^1(\nu d_{3/2})^1$	$(\pi g_{7/2})^2$ or $(\pi g_{7/2})^1(\pi d_{5/2})^1$	13^-	4
$(\nu h_{11/2})^3(\nu d_{3/2})^1$		15^-	4
$(\nu h_{11/2})^3(\nu d_{3/2})^1$	$(\pi g_{7/2})^2$ or $(\pi g_{7/2})^1(\pi d_{5/2})^1$	21^-	6
$(\nu h_{11/2})^1$	$(\pi g_{7/2})^2$ or $(\pi g_{7/2})^1(\pi d_{5/2})^1$	$23/2^-$	3
$(\nu h_{11/2})^3$		$27/2^-$	3
$(\nu h_{11/2})^5$		$35/2^-$	5
$(\nu h_{11/2})^3$	$(\pi g_{7/2})^2$ or $(\pi g_{7/2})^1(\pi d_{5/2})^1$	$39/2^-$	5
$(\nu d_{3/2})^1$	$(\pi g_{7/2})^2$ or $(\pi g_{7/2})^1(\pi d_{5/2})^1$	$15/2^+$	3
$(\nu h_{11/2})^2(\nu d_{3/2})^1$		$23/2^+$	3
$(\nu h_{11/2})^2(\nu d_{3/2})^1$	$(\pi g_{7/2})^2$ or $(\pi g_{7/2})^1(\pi d_{5/2})^1$	$35/2^+$	5
$(\nu h_{11/2})^4(\nu d_{3/2})^1$		$35/2^+$	5
$(\nu h_{11/2})^4(\nu d_{3/2})^1$	$(\pi g_{7/2})^2$ or $(\pi g_{7/2})^1(\pi d_{5/2})^1$	$47/2^+$	7

In addition, it is well known that most of the even- A Te isotopes have a vibrational behavior at low spin. With regard to the Te isotopes studied in this work, the one-phonon energy lies between 600 and 840 keV. Such an energy may compete favorably with the one involved in the successive breakings of nucleon pairs given in Table XV. Thus the yrast lines likely comprise several fragments of vibrational bands (a cascade of 2 or 3 transitions with $E_\gamma \sim 700$ keV) lying just above the fully aligned states issued from the pair breakings.

1. Evolution of states in the even- A isotopes

The systematics of the high-spin states in the $^{122-134}\text{Te}$ even- A isotopes is shown in Figs. 20(a) and 20(b).

Regarding the positive-parity states, the breaking of the proton pair shows up when $N > 76$ [see the closeness of the 6^+ and 4^+ states, drawn with diamonds in Fig. 20(a)] and the one of the first neutron pair when $N > 74$ (see the closeness of the 8^+ and 10^+ states, drawn with circles). From $N = 70$ to 78, a cascade of

two transitions of similar energies defines two states with $I^\pi = 12^+$ and 14^+ which can be interpreted as a vibrational motion above the 10^+ state [see the squares in Fig. 20(a)]. In addition, a 16^+ state has been observed in $^{126,128}\text{Te}$ which only decays towards the quasi-vibrational 14^+ level (see Figs. 2 and 4). Around 5 MeV, the group of several states with spin 13^+ , 14^+ , 15^+ , and 16^+ [see the empty diamonds in Fig. 20(a)] involves likely the breakings of one neutron pair (with $I_{max} = 10^+$) and of one proton pair (with $I_{max} = 6^+$).

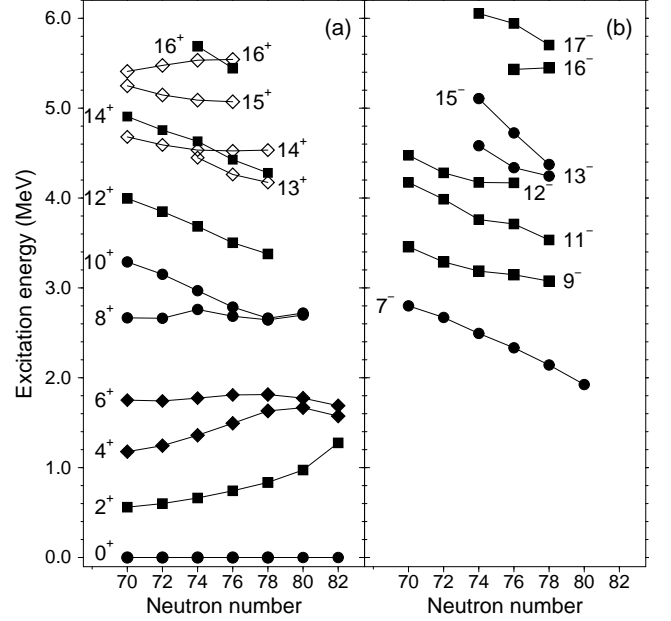


FIG. 20. Evolution of the high-spin states of the even- A Te isotopes as a function of the neutron number (this work and Ref. [43] for ^{122}Te), (a) positive-parity states, (b) negative-parity states.

The evolution of the negative-parity states is shown in Fig. 20(b). Above the well-known 7^- state having the $(\nu h_{11/2})^1(\nu d_{3/2})^1$ configuration, we expect the breaking of the proton pair (giving $I_{max} = 13^-$, see Table XV), as well as the breaking of another neutron pair (giving $I_{max} = 15^-$, see Table XV). Such configurations can be assigned to the experimental states with $I^\pi = 9^-$, 11^- , 12^- , 13^- , and 15^- . Because of the closeness of the 13^- and 15^- states in ^{128}Te , one could assume that both of them have a $(\nu h_{11/2})^3(\nu d_{3/2})^1$ configuration, as observed in $^{120-128}\text{Sn}$ [6, 7].

In summary, the closeness of the 8^+ and 10^+ states on the one hand and that of the 13^- and 15^- states on the other hand, for $N > 76$, could be interpreted in terms of pure neutron configurations. Such an assumption can be tested using the values of the transition probabilities since the $B(E2)$ reduced transitions probabilities show large values as soon as proton components are involved. Table XVI presents the characteristics of the $E2$ decay of the 10^+ state of $^{126-132}\text{Te}$ and the $B(E2)$ values are

drawn in Fig. 21(a) in comparison with those obtained in Sn isotopes.

TABLE XVI. Properties of the 10^+ isomeric states of $^{126-132}\text{Te}$.

	E_i keV	E_γ keV	$T_{1/2}^{(a)}$ ns ^(b)	$B(E2)^{(a)}$ $e^2 fm^4$	$B(E2)^{(a)}$ W.u.
^{126}Te	2972	208.1	10.7(9)	120(10)	3.2(3)
^{128}Te	2789	101.3	236(20)	85(7)	2.2(2)
^{130}Te	2664	18.5(5)	1.90(8)	85(4)	2.2(1)
^{132}Te	2723	22(1) ^(d)	3.70(9)	42(1)	1.05(3)

(a) The number in parenthesis is the error in the least significant digit shown.

(b) From Ref. [23].

(c) This work.

(d) From Ref. [30].

The behavior of the Sn isotopes is a textbook example about the effect of the gradual filling of a j subshell on the $B(E2; I_{max} \rightarrow I_{max} - 2)$ value for a j^2 configuration. A very low value is obtained at mid-shell, namely at $N = 73$. The Te isotopes do not follow the same trend, their much higher $B(E2; 10^+ \rightarrow 8^+)$ values indicate that the wave functions of both the 10^+ and 8^+ states do have proton components [30]. The slow decrease when N is increasing indicates that the proton component is decreasing when approaching the neutron magic number.

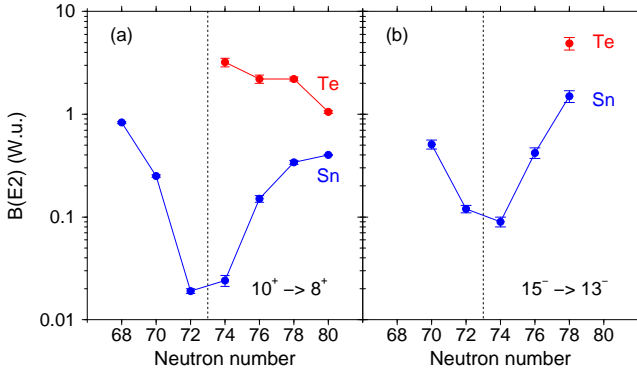


FIG. 21. (Color online) Comparison of the $B(E2)$ reduced probabilities measured in Te and Sn isotopes, (a) for the $10^+ \rightarrow 8^+$ transitions, (b) for the $15^- \rightarrow 13^-$ transitions. Experimental data are from this work and Refs. [6, 23, 30].

The reduced probabilities of the $15^- \rightarrow 13^-$ transitions are drawn in Fig. 21(b). It is worth recalling that the $B(E2; 15^- \rightarrow 13^-)$ and $B(E2; 10^+ \rightarrow 8^+)$ values are explicitly linked provided that the states have the j^3 and j^2 configuration, respectively (this is observed in Sn isotopes, see the Fig. 20 of Ref. [6]). Regarding the value measured in ^{130}Te , it is much higher than the one of ^{128}Sn , implying that the ^{130}Te states do have proton components.

2. Evolution of states in the odd- A isotopes

The evolution of the high-spin states of the odd- A Te isotopes is drawn in Figs. 22(a) and 22(b). The $23/2^-$ level is likely the fully-aligned $(\nu h_{11/2})^1 (\pi g_{7/2})^2$ state. Its excitation energy above the $11/2^-$ level increases as a function of neutron number. Such an effect is due to the residual interaction between the odd neutron and the two protons. At $N = 81$, the intensity of the interaction between the neutron hole and the proton particles is maximum, while the interaction strongly decreases at mid-shell, i.e., for $N \sim 71$. This behavior has been already pointed out in ^{49}In for the evolution of the high-spin states of the $(\nu h_{11/2})^2 (\pi g_{9/2})^1$ configuration, where the proton state is a hole [46]. Using the empirical two-body residual interactions, the evolution of the three-quasiparticle multiplet was computed as a function of the filling of the neutron orbit. Starting from mid-shell where all the states are close to each other, the decrease of the $\nu h_{11/2}$ occupation probability (in order to obtain a particle-hole configuration, such as the one of Te isotopes discussed here) leads to an increase of the energies of the highest spin states, as observed experimentally [15, 46].

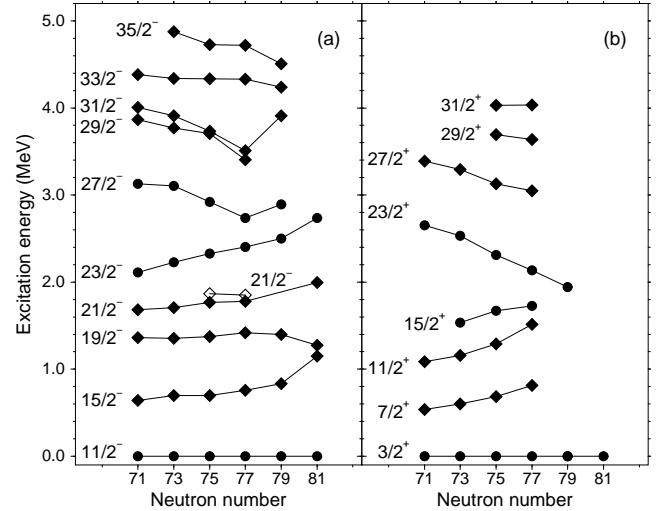


FIG. 22. Evolution of the high-spin states of the odd- A Te isotopes as a function of the neutron number (this work, Ref. [44] for ^{123}Te and Ref. [45] for ^{133}Te), (a) positive-parity states, (b) negative-parity states.

Two $21/2^-$ levels have been identified close in energy in $^{127,129}\text{Te}$ (see Figs. 14 and 16). The $21/2_2^-$ state of ^{129}Te was assigned as $(\nu h_{11/2})^1 (\pi g_{7/2})^1 (\pi d_{5/2})^1$ because it is well populated in the β decay of the high-spin isomeric state of ^{129}Sb [38]. The $21/2_2^-$ state of ^{127}Te has likely the same configuration. Regarding the $27/2^-$ level, it is likely the fully aligned $(\nu h_{11/2})^3$ state. Its excitation energy decreases as a function of the neutron number, such as the 10^+ state of the even- N isotopes. For the spin values higher than $27/2^-$, the breaking of another

pair has to be considered, either a neutron one, leading to $I_{max} = 35/2^-$, or a proton one, leading to $I_{max} = 39/2^-$ (see Table XV).

The positive-parity states are shown in Fig. 22(b). The $15/2^+$ level is due to the $(\nu d_{3/2})^1(\pi g_{7/2})^2$ configuration, while the $23/2^+$ state comes from the breaking of one $(\nu h_{11/2})^2$ pair (see Table XV). Noteworthy is the fact that the $23/2^+$ level of $^{123-129}\text{Te}$ decays towards the $21/2^-$ states by means of $E1$ transitions. As the difference in energy of these states decreases when N is increasing, the $23/2^+$ level of ^{129}Te becomes isomeric, with $T_{1/2} = 33(3)$ ns. The obtained values of the $B(E1)$ reduced transitions are of the same order of magnitude than those measured for the $7^- \rightarrow 6^+$ transition in the two neighboring even- A isotopes (see Table XVII).

TABLE XVII. Characteristics of the isomeric $E1$ transitions measured in ^{129}Te and $^{126-132}\text{Te}$.

Nucleus	E_i	E_γ	$T_{1/2}^{(a)}$	$B(E1)^{(a)}$
	keV	keV		W.u.
^{129}Te	2135.8	180	33(3) ns ^(b)	$4.7(12) \times 10^{-7}$
		251		$3.2(8) \times 10^{-7}$
^{126}Te	2495	720	0.152(5) ns ^(c)	$4.55(16) \times 10^{-6}$
^{128}Te	2336	526	2.404(24) ns ^(c)	$7.4(6) \times 10^{-7}$
^{130}Te	2145	331	110(5) ns ^(d)	$6.6(3) \times 10^{-8}$
^{132}Te	1925	151	28.1(15) μs ^(c)	$2.56(14) \times 10^{-9}$

^(a) The number in parenthesis is the error in the least significant digit shown.

^(b) From Ref. [38].

^(c) From Ref. [23].

^(d) This work.

The last point of this section is devoted to the discussion of the isomeric transition of ^{131}Te which populates the second excited state measured above the $11/2^-$ level (see Fig. 18). Using the excitation energy of the $21/2_1^-$ levels above the $11/2^-$ level in ^{129}Te and ^{133}Te [see Fig. 22(a)], we can estimate the excitation energy of the $21/2_1^-$ level in ^{131}Te , $E(21/2^-) \sim 2070$ keV. Such a value explains why the $23/2^+$ level of ^{131}Te , lying at 1943 keV, is a very-long lived isomeric state since it can only decay towards the $19/2^-$ state.

The authors of the previous work [40] had chosen an $E3$ multipolarity for the 361-keV transition, since a $M2$ multipolarity leads to a $B(M2) = 1.9 \times 10^{-6}$ W.u., a very low value as compared to those measured in Sn isotopes. Such a choice would imply that the 1580-keV state has $I^\pi = 17/2^-$. Given that no $17/2^-$ state is observed in the yrast lines of the neighboring Te isotopes, while a $19/2^-$ state is measured around this energy, the $M2$ multipolarity is much more likely. Nevertheless it is worth checking the configurations involved in the $M2$ transitions of the Sn and Te isotopes. In $^{123-127}\text{Sn}$, the main components of the initial state are $(\nu h_{11/2})^2(\nu d_{3/2})^1/(\nu h_{11/2})^2(\nu s_{1/2})^1$ and the one of the final state, $(\nu h_{11/2})^3$. The hindrance of

$M2$ transition is due to the change of the neutron orbit, $\nu d_{3/2}/\nu s_{1/2} \rightarrow \nu h_{11/2}$, implying $\Delta\ell = 3$ and $\Delta j = 4$, at least. In ^{131}Te , the main component of the $23/2^+$ state is $(\nu h_{11/2})^2(\nu d_{3/2})^1$ and the one of the $19/2^-$ state is $(\nu h_{11/2})^1(\pi g_{7/2})^2$. The $M2$ transition is then more hindered because it has to involve the change of one proton state (for the breaking of one proton pair), in addition to the one of the neutron orbit.

B. Shell-model calculations

In order to have a deeper understanding of the excitations involved in the high-spin states identified in the heavy- A Te isotopes, particularly the respective roles of the neutrons and the protons, we have performed shell-model (SM) calculations using the interaction SN100PN taken from Brown *et al* [1] which contains four parts, the proton-proton, neutron-neutron and proton-neutron interactions, the Coulomb repulsion being added to the interaction between protons. We used the shell-model code NuShellX@MSU [47]. The valence space includes five proton orbits and five neutron orbits ($g_{7/2}$, $d_{5/2}$, $d_{3/2}$, $s_{1/2}$, $h_{11/2}$), which is suitable for the description of nuclei with $Z \geq 50$ and $N \leq 82$.

We have calculated the excited states of $^{128-131}\text{Te}$ in the full space. The lightest isotopes, $^{128,129}\text{Te}$, with their numerous holes in the $N = 50 - 82$ shell, are good cases to investigate the breaking of several neutron pairs in the presence of protons. On the other hand, the calculations of more lighter isotopes would lead to too large dimensions and would need to make valence-space truncations which may lead to ambiguity in the understanding of the results.

We have also calculated, without any truncation, the excited states of $^{125-130}\text{Sn}$ isotopes using the same interaction and valence space, this allows us to test the neutron part of the SN100PN interaction.

In Sec. IV B 1, we first compare the experimental and calculated level schemes for $^{126,125}\text{Sn}$. Then in Sec. IV B 2, we discuss the results obtained for the excited states of $^{128-131}\text{Te}$. The analysis of the wave functions of some selected states allows us to determine to what extent the breaking of the proton pair affects the Te high-spin states, particularly the existence of states having the same neutron configurations as those of the Sn isotopes.

1. Description of the high-spin states of Sn isotopes

The evolution of the experimental high-spin states of the heavy Sn isotopes as a function of the neutron number is very smooth (see Figs. 19 and 21 of Ref. [6]). This feature is well described by the SM calculations done in the present work. Thus we only show two typical results, those of ^{126}Sn and ^{125}Sn .

Results of the shell-model calculations for ^{126}Sn are compared to the experimental results [6] in Fig. 23. The

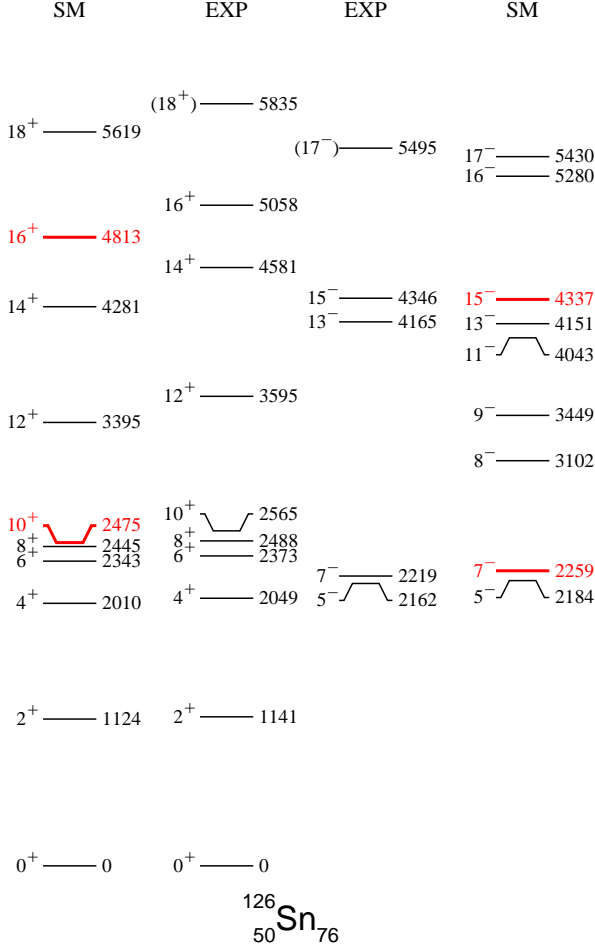


FIG. 23. (Color online) Comparison of experimental [6] and calculated high-spin states of ^{126}Sn . The SM levels drawn in red are due to the complete alignment of the angular momenta of the neutron of broken pairs (see text).

excitation energies of most of the SM states are very close to the experimental ones, only the 12^+ , 14^+ , 16^+ , and 18^+ states are predicted ~ 200 keV too low. The four SM states drawn in red, with $I^\pi = 7^-$, 10^+ , 15^- and 16^+ , are the fully aligned states of broken-pair configurations involving n neutrons in the $\nu h_{11/2}$ orbit, with $n = 1, 2, 3$ and 4 , respectively (see Table XV).

Similarly, results of the shell-model calculations for ^{125}Sn are compared to the experimental results [6, 8, 23] in Fig. 24. In this case also, the deviation between experimental and calculated energies is low, mostly below 100 keV. Regarding the positive-parity states, it is important to notice that the $15/2^+$ and $19/2^+$ levels are predicted very close to each other but in a reverse order. Moreover, even though no excited state lying above the $23/2^+$ level has yet been identified experimentally in ^{125}Sn , the excitation energy of the expected $35/2^+$ state can be estimated from the experimental results of

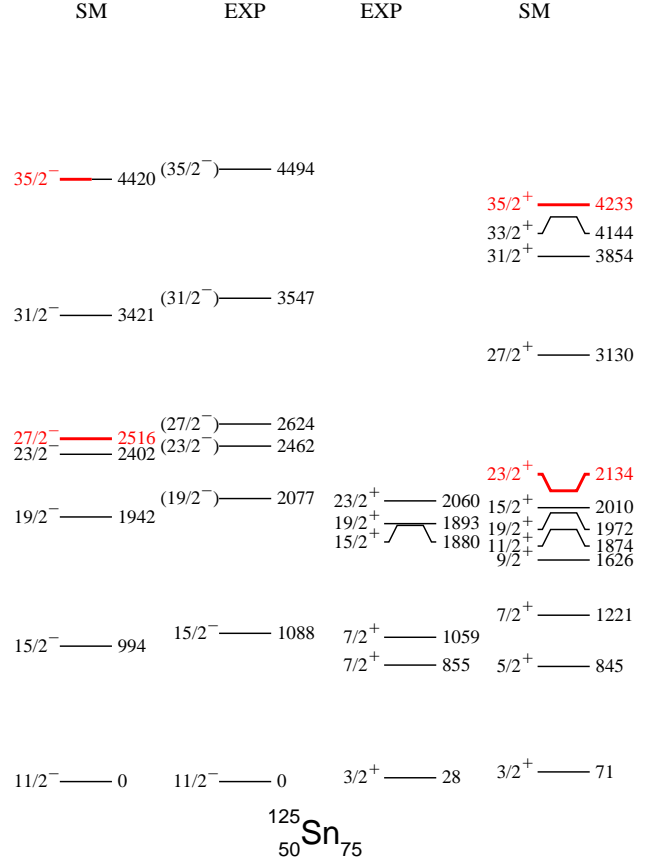


FIG. 24. (Color online) Comparison of experimental [6, 8, 23] and calculated high-spin states of ^{125}Sn . The SM levels drawn in red are due to the complete alignment of the angular momenta of the neutron of broken pairs (see text).

$^{121-123}\text{Sn}$, where the gap in energy between the $35/2^+$ and $23/2^+$ states is 2280 keV and 2225 keV, respectively [6]. This is in very good agreement with the SM prediction for ^{125}Sn , the $35/2^+$ state lying 2099 keV above the $23/2^+$ one.

The three states drawn in red, with $I^\pi = 23/2^+$, $27/2^-$ and $35/2^+$, are the fully aligned states of broken-pair configurations involving n neutrons in the $\nu h_{11/2}$ orbit, with $n = 2, 3$, and 4 , respectively (see Table XV). The $35/2^-$ state is partially drawn in red as only 60% of its wave function is the $(\nu h_{11/2})^5$ fully aligned state.

2. Description of the high-spin states of Te isotopes

a. Even-N isotopes: $^{128,130}\text{Te}$. Results of the shell-model calculations for ^{128}Te are given in Fig. 25, in comparison with the experimental results obtained in the present work. Every experimental state has a theoretical counterpart in the same energy range. The new features of the high-spin level scheme of ^{128}Te , as compared to the one of its isotone, ^{126}Sn , are well described: (i) the close-

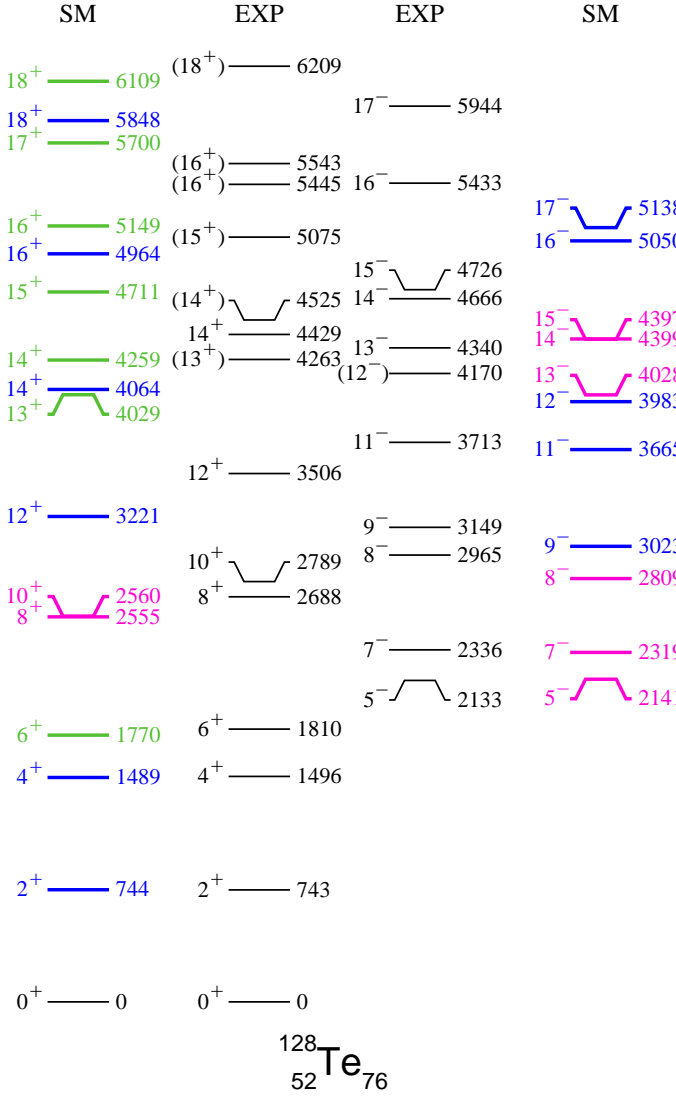


FIG. 25. (Color online) Comparison of experimental and calculated high-spin states of ^{128}Te . The major part ($\geq 50\%$) of the wave functions of the states drawn in magenta is only due to the breaking of neutron pairs ($I_p = 0$), those drawn in green have a broken proton pair with $I_p = 6$, and those drawn in blue have several components with various values of I_n and I_p (some cases are shown in Fig. 27).

ness of the 6^+ and 4^+ states, (ii) the presence of a second set of states above the 12^+ level, forming a $\Delta I = 1$ series, and (iii) the existence of the 12^- and 14^- states in the negative-parity yrast line.

Comparison of experimental and calculated levels of ^{130}Te is shown in Fig. 26. The excitation energies of most of the SM states are even much closer to the experimental ones than in the case of ^{128}Te .

The analysis of the wave functions allows us to identify which nucleon pairs are broken to obtain the total angular momentum of the calculated states. For that purpose, we use (i) the values of the two components, I_n and I_p ,

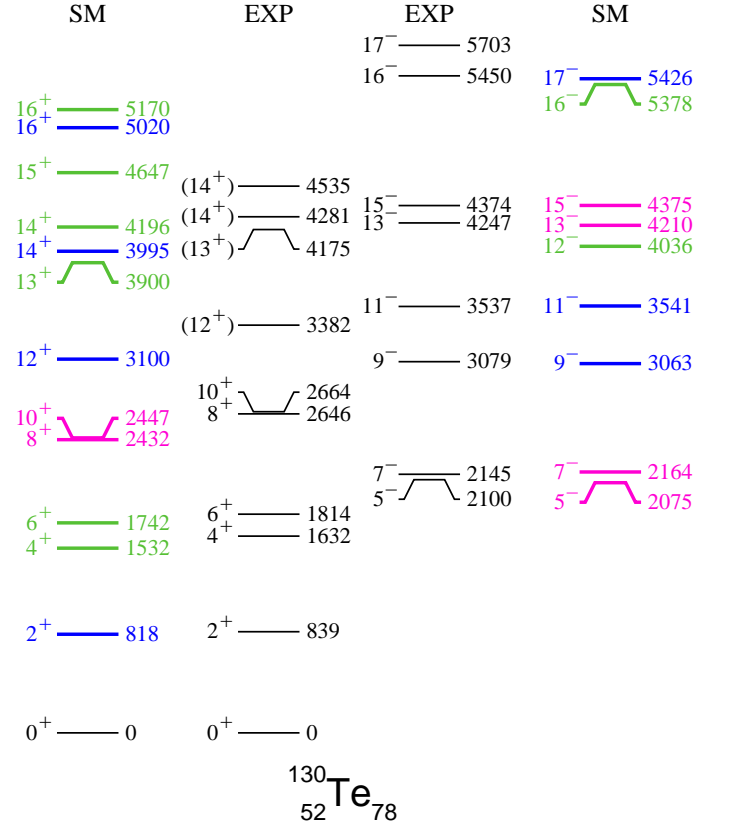


FIG. 26. (Color online) Comparison of experimental and calculated high-spin states of ^{130}Te . The color code of the SM states is the same as that of Fig. 25.

which are coupled to give the total angular momentum of each state and (ii) for each I_n and I_p component, its decomposition in terms of proton-neutron configurations, i.e., the occupation numbers of the ten valence orbits which are considered in the present calculations.

Typical results of positive-parity states of ^{128}Te are given in Figs. 27(a)–27(d). The major component (62%) of the 10^+ state predicted at 2560 keV comes from the breaking of the neutron pair ($I_n = 10$), the two protons being paired ($I_p = 0$). Such a feature does not hold for the 12^+ state predicted at 3221 keV, where the component corresponding to the breaking of the neutron pair ($I_n = 12$), the two protons being paired ($I_p = 0$), is only 38%, while another large component (32%) involves the breaking of both neutron and proton pairs. The comparison of the wave functions of the two 14^+ states is very instructive. The 14_1^+ state calculated at 4064 keV shows many components, while the 14_2^+ state calculated at 4259 keV has mainly $I_p = 6$ (with $I_n = 8-12$), i.e., the proton pair being broken and the two angular momenta being fully aligned. In summary, the positive-parity states of ^{128}Te given in Fig. 25 can be sorted in three families drawn with three colors. The major part

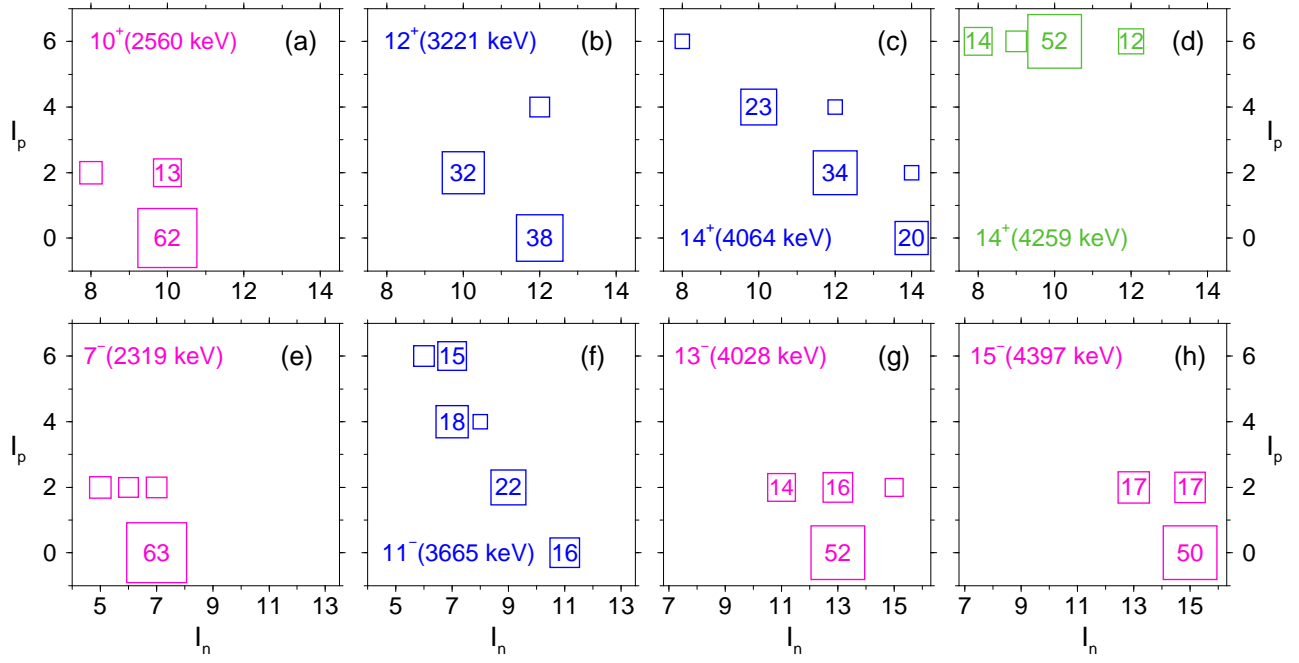


FIG. 27. (Color online) Decomposition of the total angular momentum of selected states of ^{128}Te into their $I_n \otimes I_p$ components. The percentages above 10% are written inside the squares, drawn with an area proportional to it. Percentages below 5% are not written. The color code is the same as the one of Fig. 25. (a)–(d) positive-parity states, (e)–(h) negative-parity states.

($\geq 50\%$) of the wave functions of the states drawn in magenta is only due to the breaking of a neutron pair ($I_p = 0$), this is the case of the 8^+ and 10^+ states. Those drawn in green have the broken proton pair with $I_p = 6$, such as the 6^+ calculated at 1770 keV and the set of $\Delta I = 1$ states, from 13^+ to 18^+ . Finally, those drawn in blue have several components with various values of I_n and I_p , such as the 2^+ , 4^+ , 12^+ states, as well as the set of $\Delta I = 2$ states, from 14^+ to 18^+ . Because of their large numbers of components, these levels resemble ‘collective’ states. Finally, it is important to note that the SM calculations give a coherent picture of the two structures measured above the 12_1^+ states in the even- N Te isotopes.

The components of typical negative-parity states of ^{128}Te are given in Figs. 27(e)–27(h). The major component (63%) of the 7^- state predicted at 2319 keV comes from the breaking of the neutron pair ($I_n = 7$), the two protons being paired ($I_p = 0$). The 13^- state predicted at 4028 keV and the 15^- state (4397 keV) also have their major component (52% and 50%, respectively) coming from the breaking of neutron pairs ($I_n = 13$ and 15 , respectively), the two protons being paired ($I_p = 0$). On the other hand, the 11^- state calculated at 3665 keV shows many components. The negative-parity states of ^{128}Te given in Fig. 25 can then be sorted in two families, the major part ($\geq 50\%$) of the wave function of states drawn in magenta is due to the breaking of a neutron pair ($I_p = 0$) while the states drawn in blue have several components with various values of I_n and I_p .

TABLE XVIII. Comparison of the experimental and calculated values of $B(E2)$ for transitions de-exciting isomeric states in $^{128,130,132}\text{Te}$.

Nucleus	$J_i^\pi \rightarrow J_f^\pi$	$B_{exp}(E2)^{(a)}$ $e^2 fm^4$	$B_{SM}(E2)$ $e^2 fm^4$
^{128}Te	$10^+ \rightarrow 8^+$	85(7)	110
^{130}Te		85(4)	154
^{132}Te		42(1)	30
^{128}Te	$15^- \rightarrow 13^-$	-	274
^{130}Te		193(29)	135

^(a) The number in parenthesis is the error in the least significant digit shown.

b. Odd- N isotopes: $^{129,131}\text{Te}$. The negative-parity yrast line predicted in $^{129,131}\text{Te}$ (see Figs. 28 and 29) exhibits several new high-spin states as compared to the one of the odd- N Sn isotopes, such as the $21/2^-$ level lying above the $19/2^-$ one, or the $29/2^-$ and $33/2^-$ levels lying between the $31/2^-$ and $35/2^-$ ones. This is in good agreement with the experimental results. All the calculated levels of $^{129,131}\text{Te}$ show the same sequence as the experimental ones and have an energy in the right energy range. Nevertheless it is important to notice that the differences between the experimental and calculated excitation energies can amount up to ~ 400 keV in ^{129}Te , its SM level scheme being more compressed than the experimental one.

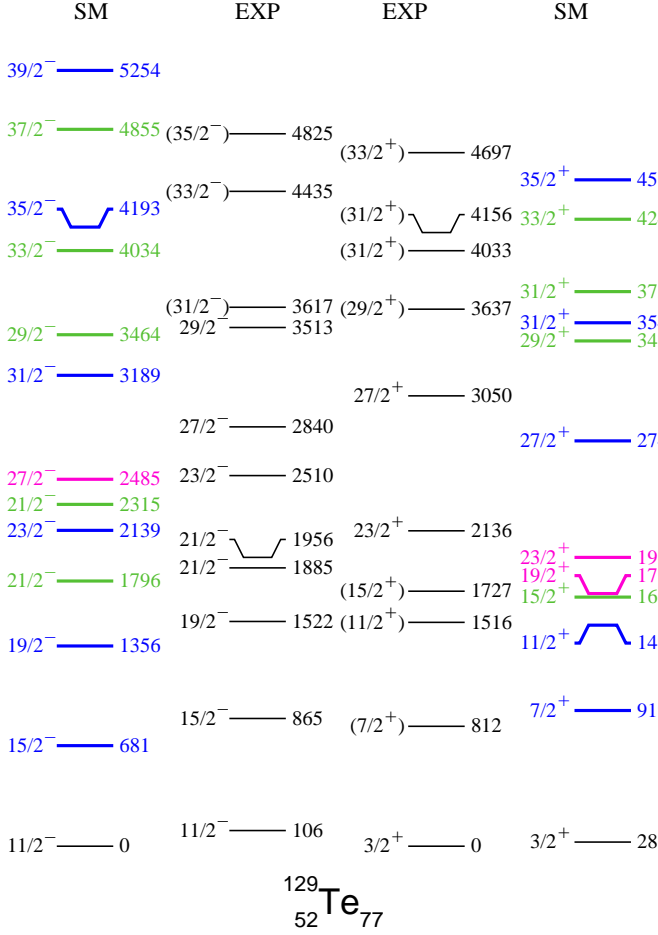


FIG. 28. (Color online) Comparison of experimental and calculated high-spin states of ^{129}Te . The color code of the SM states is the same as that of Fig. 25.

The components of typical negative-parity states of ^{129}Te are given in Figs. 30(a)–30(d). All the components of the $21/2^-$ state predicted at 1796 keV come from the breaking of the proton pair ($I_p = 6$), and the major component (63%) has one odd neutron in the $h_{11/2}$ orbit ($I_n = 11/2$). The major component (55%) of the $27/2^-$ state predicted at 2485 keV comes from the breaking of a neutron pair ($I_n = 27/2$), the two protons being paired ($I_p = 0$). Above the $27/2^-$ state, two sets of states are predicted to coexist in the same energy range. The wave function of the $31/2^-$ state calculated at 3189 keV displays many components with various values of both I_p and I_n (similar results are obtained for the $35/2^-$ state at 4193 keV and the $39/2^-$ state at 5254 keV). On the other hand, the components of the $29/2^-$ state calculated at 3464 keV come mainly from the breaking of the proton pair ($I_p = 6$). The same is observed for the $33/2^-$ state at 4034 keV and the $37/2^-$ state at 4855 keV.

The components of typical positive-parity states of ^{129}Te are given in Figs. 30(e)–30(h). The main com-

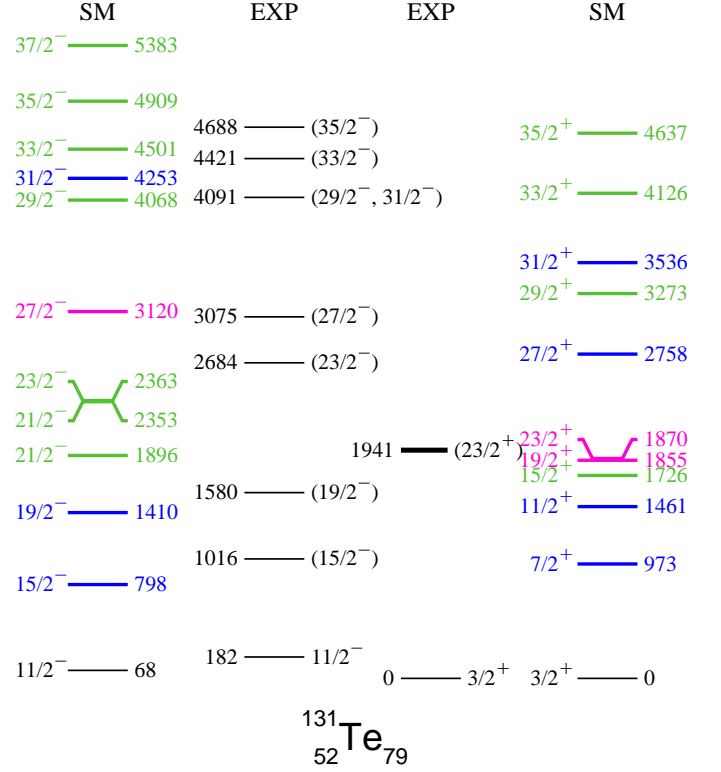


FIG. 29. (Color online) Comparison of experimental and calculated high-spin states of ^{131}Te . The color code of the SM states is the same as that of Fig. 25.

ponents of the $15/2^+$ state calculated at 1687 keV come from the breaking of the proton pair ($I_p = 6$), and the major component (64%) has one odd neutron in the $d_{3/2}$ orbit ($I_n = 3/2$). Less than 300 keV above, the $23/2^+$ state has a major component (59%) coming from the breaking of a $\nu h_{11/2}$ pair ($I_n = 23/2$ and $I_p = 0$). The two sets of states predicted above the $23/2^+$ have different configurations. The $27/2^+$ level exhibits many components with various values of both I_p and I_n (similar results are obtained for the $31/2^+$ state at 3545 keV and the $35/2^+$ state at 4513 keV), while the components of the $29/2^+$ state calculated at 3422 keV come mainly from the breaking of the proton pair ($I_p = 6$), as the ones of the $31/2^+$ and $33/2^+$ states.

In summary, the calculated states of $^{129,131}\text{Te}$ given in Figs. 28 and 29 can be sorted in three families drawn with the same colors as used for $^{128,130}\text{Te}$. The breaking of the first neutron pair leads to the major component of the $19/2^+$, $23/2^+$, and $27/2^-$ states. Two sets of states are predicted to coexist above them. The levels of one set (drawn in blue) have many components, resembling ‘collective’ states, while all the levels of the other one (drawn in green) have mainly a broken proton pair.

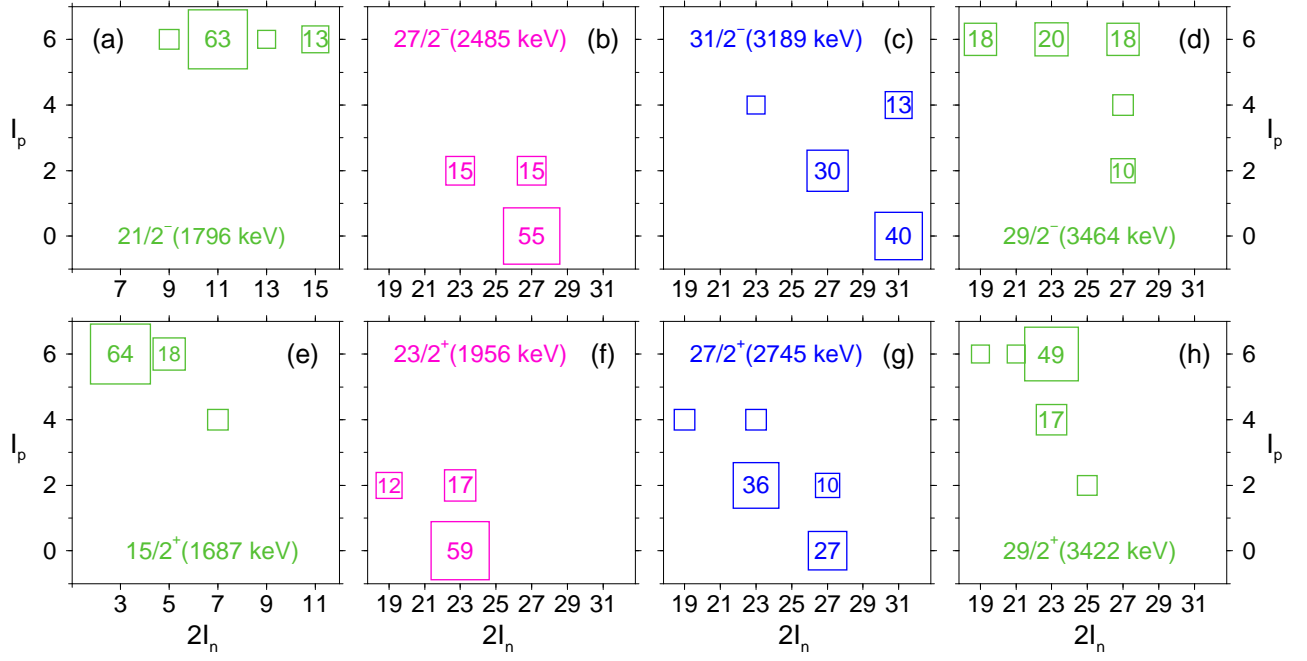


FIG. 30. (Color online) Decomposition of the total angular momentum of selected states of ^{129}Te into their $I_n \otimes I_p$ components. The percentages above 10% are written inside the squares, drawn with an area proportional to it. Percentages below 5% are not written. The color code is the same as the one of Fig. 28. (a)–(d) negative-parity states, (e)–(h) positive-parity states.

3. Conclusion

The neutron part of the SN100PN effective interaction gives a very good description of the high-spin states of the heavy Sn isotopes. The agreement between the calculated and experimental energies of the excited states of the heavy Te isotopes is slightly less good, the predicted level schemes being too compressed as compared to the experimental results. One could suspect that the values of some proton-proton two-body matrix elements (TBME) are slightly too attractive, as similar features were observed previously in several $N = 82$ isotones, where only such TBME are active. It is worth recalling that the SN100PN interaction has been recently used [3] to calculate their high-spin states which were measured previously [2]. The theoretical levels schemes of ^{137}Cs , ^{138}Ba , ^{139}La , and ^{140}Ce display the same sequences as the experimental ones, but some high-spin states are predicted too low in energy (by an amount from ~ 200 keV to 400 keV).

Noteworthy is the fact that only the fully aligned states corresponding to the breaking of one neutron pair in the $h_{11/2}$ orbit (see the cases written in bold in Table XV) are observed in the heavy- A Te isotopes. On the other hand, the main configurations of all the higher spin states contain the breaking of the proton pair. This is at variance with the Sn isotopes where the breaking of two and three neutron pairs are identified [6].

V. SUMMARY

In this work, the $^{124-131}\text{Te}$ isotopes were produced in two fusion-fission reactions, $^{18}\text{O}+^{208}\text{Pb}$ and $^{12}\text{C}+^{238}\text{U}$, and the emitted γ rays were detected by the Euroball array. A fragment detector was also associated to the γ -ray detection, in another experiment. All the data sets recorded in these experiments have allowed us to extend the level schemes of $^{124-131}\text{Te}$ isotopes to higher spins ($\sim 17h$) and higher excitation energies ($\sim 5 - 6$ MeV). Furthermore, the performed $\gamma - \gamma$ angular correlations supported the former spin assignments in most cases and yielded about 30 new spin assignments. The half-lives of three isomeric states were measured, showing that the decay of the 10^+ state of ^{128}Te is much faster than reported in the last compilation. In addition, the unexpected production of heavier- A Te nuclei as well as of some isotopes of Xe, Ba, and Ce was discussed in terms of transfer/incomplete fusion in the $^{12}\text{C}+^{238}\text{U}$ reaction, thanks to the unambiguous identification of their complementary fragments.

The high-spin structures of the $^{124-131}\text{Te}$ have been first discussed in comparison with the general features known in the mass region. Then shell-model calculations using the SN100PN effective interaction have been successfully compared to experimental results. Thanks to the I_n and I_p components of the SM wave functions, the effect of the proton-pair breaking has been identified. The fully aligned component with $I_p = 6$ shows up clearly by the appearance of sets of excited levels, for instance

above the $(\nu h_{11/2})^2 10^+$ state in the even- N isotopes and the $(\nu h_{11/2})^3 27/2^-$ state in the odd- N ones.

ACKNOWLEDGMENTS

The Euroball project was a collaboration among France, the United Kingdom, Germany, Italy, Denmark and Sweden. The first experiment has been performed

under U.E. contract (ERB FHGECT 980 110) at Legnaro. The second experiment has been supported in part by the EU under contract HPRI-CT-1999-00078 (EURO-VIV). We thank many colleagues for their active participation in the experiments, Drs. A. Bogachev, A. Buta, J.L. Durell, Th. Ethvignot, F. Khalfalla, I. Piqueras, A.A. Roach, A.G. Smith and B.J. Varley. We thank the crews of the Vivitron. We are very indebted to M.-A. Saettle for preparing the Pb target, P. Bednarczyk, J. Devin, J.-M. Gallone, P. Médina, and D. Vintache for their help during the experiment.

-
- [1] B.A. Brown, N.J. Stone, J.R. Stone, I.S. Towner and M. Hjorth-Jensen, *Phys. Rev. C* **71**, 044317 (2005).
- [2] A. Astier *et al.*, *Phys. Rev. C* **85**, 064316 (2012).
- [3] P.C. Srivastava, M.J. Ermamatov and I. O. Morales, *J. Phys. G: Nucl. Part. Phys.* **40**, 035106 (2013).
- [4] C. T. Zhang *et al.*, *Nucl. Phys.* **A628**, 386 (1998).
- [5] R. Broda *et al.*, *Eur. Phys. J. A* **20**, 145 (2004).
- [6] A. Astier *et al.*, *Phys. Rev. C* **85**, 054316 (2012).
- [7] S. Pietri *et al.*, *Phys. Rev. C* **83**, 044328 (2011).
- [8] R. Lozeva *et al.*, *Phys. Rev. C* **77**, 064313 (2008).
- [9] J. Simpson, *Z. Phys. A* **358**, 139 (1997) and F. A. Beck *Prog. Part. Nucl. Phys. A* **28**, 443 (1992).
- [10] J. Eberth *et al.*, *Nucl. Instrum. Methods A* **369**, 135 (1996).
- [11] G. Duchêne *et al.*, *Nucl. Instrum. Methods A* **432**, 90 (1999).
- [12] D. Radford, *Nucl. Instrum. Methods A* **361**, 297 and 306 (1995).
- [13] M.A.C. Hotchkis *et al.*, *Nucl. Phys.* **A530**, 111 (1991).
- [14] M.-G. Porquet *et al.*, *Acta Phys. Polonica B* **27**, 179 (1996).
- [15] R. Lucas *et al.*, *Eur. Phys. J. A* **15**, 315 (2002).
- [16] M.-G. Porquet *et al.*, *Eur. Phys. J. A* **24**, 39 (2005).
- [17] Ch. Theisen *et al.*, *Proceedings of the 2nd International Workshop on Nuclear Fission and Fission Product Spectroscopy, Seyssins, France*, April 1998, AIP Conf. Proc. **447**, 143 (1998).
- [18] A. Astier *et al.*, *Eur. Phys. J. A* **30**, 541 (2006).
- [19] M.-G. Porquet *et al.*, *Phys. Rev. C* **84**, 054305 (2011).
- [20] A. Astier *et al.*, *Phys. Rev. C* **88**, 024321 (2013).
- [21] N. Warr *et al.*, *Nucl. Phys.* **A636**, 379 (1998).
- [22] A. Kerek, *Nucl. Phys.* **A176**, 466 (1971).
- [23] ENSDF database, <http://www.nndc.bnl.gov/ensdf/>.
- [24] A.M. Bruce *et al.*, *Phys. Rev. C* **55**, 620 (1997).
- [25] F.R. Xu, P.M. Walker, and R. Wyss, *Phys. Rev. C* **59**, 731 (1999).
- [26] A. Kerek, *Nucl. Phys.* **A185**, 497 (1972).
- [27] M. Houry, Thesis, Université Paris-Sud, Orsay, 2000, Saclay Report No. DAPNIA/SPHN-00-01-T.
- [28] M. Kanbe and K. Kitao, *Nuclear Data Sheets* **94**, 227 (2001).
- [29] A. Kerek, P. Carlé, and J. McDonald, *Nucl. Phys.* **A198**, 466 (1972).
- [30] J. Genevey *et al.*, *Phys. Rev. C* **63**, 054315 (2001).
- [31] M. Houry *et al.*, *Proceedings of the 2nd International Workshop on Nuclear Fission and Fission Product Spectroscopy, Seyssins, France*, April 1998, AIP Conf. Proc. **447**, 220 (1998).
- [32] T. Kibédi *et al.*, *Nucl. Instrum. Methods A* **589**, 202 (2008).
- [33] A. Kerek, J. Kownacki, A. Marekius and J. Pihl, *Nucl. Phys.* **A194**, 64 (1972).
- [34] J. Katakura, *Nuclear Data Sheets* **112**, 1647 (2011).
- [35] A. Hazhizume, *Nuclear Data Sheets* **112**, 495 (2011).
- [36] H. Huck, M.L. Pérez and J.J. Rossi, *Phys. Rev. C* **26** 621 (1982).
- [37] C.A. Stone and W.B. Walters, *Z. Phys. A* **328**, 257 (1987).
- [38] C. T. Zhang *et al.*, *Z. Phys. A* **353**, 11 (1995).
- [39] Y. Tendow, *Nuclear Data Sheets* **77**, 631 (1996).
- [40] B. Fogelberg *et al.*, *Proceedings of the 2nd International Workshop on Nuclear Fission and Fission Product Spectroscopy, Seyssins, France*, April 1998, AIP Conf. Proc. **447**, 191 (1998).
- [41] C. T. Zhang *et al.*, *Phys. Rev. Lett.* **77**, 3743 (1996).
- [42] A. Korgul *et al.*, *Eur. Phys. J. A* **7**, 167 (2000).
- [43] E.S. Paul, D.B. Fossan, G.J. Lane, J.M. Sears, I. Thorslund, and P. Vaska, *Phys. Rev. C* **53** 1562 (1996).
- [44] N. Blasi *et al.*, *Z. Phys. A* **354**, 233 (1996).
- [45] P. Bhattacharyya *et al.*, *Phys. Rev. C* **64** 054312 (2001).
- [46] M.-G. Porquet *et al.*, *Eur. Phys. J. A* **20**, 245 (2004).
- [47] B.A. Brown, W.D.M. Rae, E. McDonald and M. Horoi, NuShellX@MSU, <http://www.nscl.msu.edu/~brown/resources/resources.html>.